Titre: Title:	Charge Carrier Transport in Amorphous Glassy Organic Semiconductors
Auteur: Author:	Zhaojing Gao
Date:	2022
Type:	Mémoire ou thèse / Dissertation or Thesis
Référence: Citation:	Gao, Z. (2022). Charge Carrier Transport in Amorphous Glassy Organic Semiconductors [Thèse de doctorat, Polytechnique Montréal]. PolyPublie. https://publications.polymtl.ca/10510/

POLYTECHNIQUE MONTRÉAL

affiliée à l'Université de Montréal

Charge carrier transport in amorphous glassy organic semiconductors

ZHAOJING GAO

Département de génie physique

Thèse présentée en vue de l'obtention du diplôme de *Philosophiæ Doctor*

Génie des matériaux

Juillet 2022

POLYTECHNIQUE MONTRÉAL

affiliée à l'Université de Montréal

Cette thèse intitulée :

Charge carrier transport in amorphous glassy organic semiconductors

présentée par **Zhaojing GAO**

en vue de l'obtention du diplôme de *Philosophiæ Doctor*

a été dûment acceptée par le jury d'examen constitué de :

Jolanta-Ewa SAPIEHA, présidente
Clara SANTATO, membre et directrice de recherche
Arthur YELON, membre et codirecteur de recherche
Michael WERTHEIMER, membre
Emanuele ORGIU, membre externe

ACKNOWLEDGEMENTS

My sincerely appreciation goes first and foremost to Professor Clara Santato, my supervisor, for helping me out of all difficulties and supporting without any complaint in both the research and life. She has accompanied me all the steps of writing my thesis. Whenever I need help with my research, she is always available. My deepest and profound acknowledgement goes to Professor Arthur Yelon, my co-supervisor, for his wonderful inspiration and extremely professional guidance. Without his consistent instruction, this thesis could not have been accomplished. As the most ordinary girl in the research field, sometimes I feel frustrated and confused. But at every moment, my two supervisors are always with me. Their enthusiasm and patience to the research have a great influence on me.

I also need to thank my colleagues: Arun, Dieudonné, Tian, Manuel, Anthony, Xiang, Shiming, Yang, Ramin, Orlando, Molood, Yasser, Shahid for their help and support during my research. It is very pleasure to work with you. Many thanks to Yves Drolet and Christophe Clément for their technical assistance during my experiments.

Futhermore, I would like to express special gratitude to my jury members: Professor Jolanta-Ewa Sapieha, Professor Michel Wertheimer and Professor Emanuele Orgiu for volunteering their time to read this thesis.

Finally, I would like to thank my beloved families and friends for their unconditional support.

RÉSUMÉ

Les polymères et petites molécules semi-conducteurs organiques ont été largement étudiés, en raison de leur possible traitement en solution (imprimabilité), de leur compatibilité avec des substrats flexibles et de leurs propriétés optoélectroniques ajustables par la synthèse chimique. Cependant, ils présentent de fortes concentrations de défauts qui entraînent des désordres structurels et énergétiques, difficiles à éliminer, résultats de faibles interactions intermoléculaires aussi appelées forces de van der Waals. Le fort couplage porteur de charge-phonon, c'est-à-dire un électron ou trou couplé à un phonon, ainsi que le désordre dans les semi-conducteurs organiques conduisent à la localisation des porteurs de charge et à la formation de polarons. Celles-ci conduisent ainsi à la difficulté de comprendre les mécanismes détaillés du transport des porteurs de charge dans les matériaux organiques.

Dans cette thèse, les mécanismes de conduction dans les semi-conducteurs organiques sont étudiés à travers le comportement de Meyer Neldel (MN). Les effets de la température T, du champ électrique, du poids moléculaire et de la fréquence du courant alternatif (CA) sur le transport sont étudiés.

Les mécanismes de transport des porteurs de charge dans le Poly(3-hexylthiophène-2,5-diyl) (P3HT) regio-régulier, avec trois poids moléculaires différents, glacé amorphe sont déterminés sans ambiguïté, à la fois en-dessous et au-dessus de la température T_α, dite la température de transition à l'état glacé amorphe. Ceci est le résultat de mesures de la température, du champ électrique et de la dépendance en fréquence alternative de la mobilité et de la densité des porteurs de charge dans des transistors à effet de champ sur le P3HT. Les relaxations moléculaires jouent un rôle important dans la conductivité en courant continu. À des températures supérieures à T_α, sous une tension drain-source constante, les porteurs polaroniques sous forme de trous sont transportés avec chaines de polymères mobiles et peuvent sauter d'une chaine à l'autre. En dessous de T_α, ils sautent entre des segments de chaînes mobiles de molécules voisines essentiellement immobiles. En appliquant des tensions drain-source alternatives à des fréquences supérieures ou égales à 100 Hz, les porteurs de charge sont transportés le long des chaînes de polymères. Ce mouvement le long des chaînes ne contribue pas à la conductivité en courant continu. Nous présentons le premier rapport d'un effet positif des relaxations moléculaires, mouvement de

chaines moléculaire et des segments de polymère, sur les processus de transport de porteurs de charge dans les semi-conducteurs organiques.

Comparés aux semi-conducteurs organiques de type p de haute performance, les matériaux de type n sont plus insaisissables en raison du piégeage d'électrons à l'interface et du problème d'injection de porteurs de charge au niveau des électrodes. Nous avons fabriqué des transistors à effet de champ organiques à base de PCBM (Phenyl-C61-Butyric Acid Methyl Ester) et amélioré les performances du dispositif en réduisant le piégeage d'électrons à l'interface diélectrique-semi-conducteur et en améliorant l'injection de porteurs de charge grâce aux nanotubes de carbone intégrés dans l'électrode d'or. Ces procédures ont par conséquent amélioré la mobilité des porteurs de charge des dispositifs jusqu'à trois ordres de grandeur de plus, comparé au PCBM déposé sur un substrat conventionnel de SiO_2 avec une électrode en or non traité. Le mécanisme de transport des porteurs de charge dans un PCBM a ensuite été étudié. La courbe d'Arrhenius a été utilisée pour éclairer les mécanismes de transport des porteurs de charge dans les couches minces PCBM. La cristallisation du PCBM a été observée pendant la mesure, donnant lieu à la facilité de sauts de porteurs de charge dans des régions plus cristallisées.

Ces connaissances sur la dépendance des propriétés de transport des porteurs de charge aux propriétés moléculaires devraient contribuer aux progrès des cellules photovoltaïques organiques stables, de la thermoélectronique organique et de l'électronique thermiquement dégradable. L'approche adoptée ici devrait également être utile pour clarifier les mécanismes de conduction dans d'autres semi-conducteurs à base de polymères et de petites molécules.

ABSTRACT

Organic semiconducting polymers and small molecules have been widely investigated, due to their solution processability (printability), compatibility with flexible substrates and optoelectronic properties tunable with chemical synthesis. However, they have high concentrations of defects that bring about structural and energetic disorder, difficult to eliminate, due to their weak van der Waals intermolecular interactions. Strong charge carrier-phonon coupling and disorder in organic semiconductors lead to charge carrier localization and to the formation of polarons. These lead to the difficulty in understanding detailed mechanisms of charge carrier transport in organic materials.

In this thesis, the conduction mechanisms in organic semiconductors are studied through the Meyer Neldel (MN) behavior. The effect of temperature, *T*, electrical field, molecular weight and alternating current (AC) frequency on transport are studied.

The charge carrier transport mechanisms in amorphous glassy Poly(3-hexylthiophene-2,5-diyl) (P3HT) are determined unambiguously, both below and above the glass transition temperature, T_α. This is the result of measurements of temperature, electric field, and ac frequency dependence of charge carrier mobility and density in organic field effect transistors, based on regioregular P3HT of three different molecular weights. Relaxations play an important role in dc conductivity. At temperatures above T_α, under constant drain-source voltage, the hole-like polaronic charge carriers hop between, and move with, mobile polymer chains. Below T_α, they hop between mobile chain segments of essentially immobile neighboring molecules. Under drain-source voltages at AC frequencies of 100 Hz and higher, charge carriers move along polymer backbones. This motion along the backbones does not contribute to dc conductivity. A positive effect of molecular relaxations, the movement of the molecular backbone and of chain segments on charge carrier transport processes in organic semiconductors, has not previously been reported.

Compared with high performance p-type organic semiconductors, n-type materials are more elusive, due to the electron trapping at the interface and the problem of charge carrier injection from the electrodes. We have fabricated PCBM based organic field effect transistors and improved device performance by reducing the electron trapping at the dielectric-semiconductor interface and improving charge carrier injection, using carbon nanotubes integrated into the gold electrode to improve injection efficiency. These procedures improved charge carrier mobility of the devices by

about three orders of magnitude compared to PCBM deposited on untreated SiO_2 substrate with gold electrodes. The charge carrier transport mechanism in a PCBM was then studied. Arrhenius plot has been employed to cast light on the charge carrier transport mechanisms in PCBM thin films. Crystallization of PCBM was observed during the measurement, the charge carrier hopping is then facilitated by the formation of more crystallized regions.

These insights into the dependence of charge carrier transport properties upon the molecular properties should contribute to advances in stable organic photovoltaics, organic thermoelectrics, and thermally degradable electronics. The approach taken here should also be useful for clarifying conduction mechanisms in other polymer- and small molecule-based semiconductors.

TABLE OF CONTENTS

LIST OF TABLES

LIST OF FIGURES

LIST OF SYMBOLS AND ABBREVIATIONS

A	Area
AC	Alternating current
AFM	Atomic force microscopy
Au	Gold
BCB	Divinyl tetramethyl siloxane-bis(benzocyclobutene) derivative
BSE	Backscattered electron
C	Capacitance
C_{60}	Fullerene
Ca	Calcium
CBH	Correlated barrier hopping
C_i	Specific capacitance per unit area of the gate insulator
CNT	Carbon nanotube
d	Interplanar spacing of the crystals
d	Thickness of the dielectric
DC	Direct current
DI	De-ionized
DMA	Dynamic Mechanical Analysis
DSC	Differential Scanning Calorimetry
e	Elementary charge
E’	Storage modulus
E’’	Loss modulus
E_C	Energy of the conduction band edge

E_{MN}	Meyer Neldel energy
E_T	Energy of the trap depth
$E_x(x)$	Electric field applied in x direction
f	Frequency
$\hbar\upsilon$	Excitation energy
HMDS	Hexamethyldisilazane
HOMO	Highest occupied molecular orbital
HT-HT	Head-tail head-tail
I_d	Drain source current
IPA	Isopropyl alcohol
K	A material specific constant
L	Channel length of the transistor
LUMO	Lowest unoccupied molecular orbital
MEE	Multi excitation entropy
Mg	Magnesium
MgO	Magnesium Oxide
MN	Meyer Neldel
MNE	Meyer Neldel energy
MNR	Meyer Neldel Rule
MW	Molecular weight
n	Charge carrier density
N_2	Nitrogen
N_T	Effective density of states for the trap sites
OFET	Organic field-effect transistor

OLED	Organic light-emitting diode
OPV	Organic photovoltaic cell
OTFT	Organic thin-film transistor
P3HT	Poly(3-hexylthiophene-2,5-diyl)
PCBM	Phenyl-C61-butyric acid methyl ester
PR	Photoresist
PTEN-H	N-annulated perylene tetraester
PTFE	Polytetrafluoroethylene
Q	Charge carrier density
$Q(x)$	Charge carrier density in x direction
r	Hopping distance
R	Resistance
rms	root mean square roughness
Rq	Roughness factor
RR	Regioregular
SEM	Scanning electron microscopy
SiO_2	Silicon dioxide
SWCNT	Single-wall carbon nanotube
tan δ	Mechanical damping factor
T	Temperature
T_α	Alpha relaxation temperature
$T_{\alpha,\infty}$	Alpha relaxation temperature at infinite molecular weight limit
T_c	Characteristic temperature of the assumed trap density distribution

T_g	Glass transition temperature
T_{iso}	Isokinetic temperature
Ti	Titanium
T_{MN}	Meyer Neldel temperature
V_d	Drain source voltage
V_g	Gate voltage
V_{th}	The threshold voltage
W	Channel width of the transistor
WLF	Williams-Landel-Ferry
X	Observable such as charge carrier mobility
X_0	Activation prefactor
X_{00}	Activation prefactor
XRD	X-ray diffraction
z	Variable parameter such as gate voltage
ΔE	Activation energy
ε	Vacuum permittivity
θ	Angle of incidence
k_B	Boltzmann constant
κ	Coupling constant between electrons and phonons
k	Dielectric constant
λ	Wavelength
μ	Charge carrier mobility
μ_0	Band transport mobility

μ_{eff}	Effective mobility
ρ_0	Trap density
σ	Conductivity
σ_{ac}	AC conductivity
σ_{dc}	DC conductivity
ω	Relaxation frequency
ω_g	Relaxation frequency at glass transition temperature

LIST OF APPENDICES

CHAPTER 1 INTRODUCTION

1.1 Organic semiconductors

The history of organic semiconductors began in 1970s, with the discovery of conducting polymers and their properties.[1] Since then, organic semiconducting polymers and small molecules have been widely investigated. [2, 3] The properties of organic semiconducting materials can be tuned through changing their chemical structures, which results in a great variety of organic materials. [4, 5] Thus, such materials can be versatile, to meet different demands in applications such as organic thin-film transistors (OTFTs), organic photovoltaics (OPV) and organic light-emitting diodes (OLEDs).

Compared to conventional crystalline semiconductors, organic semiconductors are characterized by lower mobility, with a benchmark value between 15 cm^2/Vs and 20 cm^2/Vs for p-type materials,[6, 7] 10 cm^2/Vs for n-type materials.[7] Although the mobility of the conventional covalent semiconductors can be several orders of magnitude higher than organic semiconductors, e.g. ca. 1400 cm^2/Vs for crystalline silicon[8] and ca. 10^7 cm^2/Vs for gallium arsenide,[9] any structure change will greatly affect their charge carrier transport, and thus deteriorate the mobility. Organic semiconducting materials have advantages such as low temperature manufacturing, solution processability and compatibility with flexible substrates.[3, 5, 10] These make them to be interesting candidates for printed electronics.[11, 12]

Unlike crystalline inorganic materials presently in use, organic semiconductors have high concentrations of defects that bring about structural and energetic disorder, difficult to eliminate, due to their weak van der Waals interactions. Strong charge carrier-phonon coupling and disorder in organic semiconductors lead to charge carrier localization and to the formation of polarons.[2] These consist of the charge carrier coupled to structural deformation, which results in effective mass much larger than that of free electrons, and further lowers the charge carrier mobility compared with that expected for charge carriers with effective mass close to the free electron (hole) mass. Although various transport models, including band-like transport,[13] multiple trap and release,[14] variable range hopping,[15] and percolation have been proposed,[16] the detailed mechanisms of charge carrier transport in organic materials are still not well understood. The dependence of electronic properties upon the molecular properties (e.g. molecular relaxations) has rarely been explained unambiguously.

1.2 Motivation

The motivation of this thesis is to use Meyer Neldel (MN) behavior (a set of comparable samples exhibit kinetic behavior independent of the activation energy at an isokinetic temperature, please see Chapter 3.1) to cast light on conduction mechanisms in organic semiconductors. The effect of temperature, *T,* electrical field, molecular weight and alternating current (AC) frequency are all studied.

The inherent disorder and strong charge carrier-phonon cooupling in organic semiconductors lead to the difficulty in understanding their charge carrier transport mechanisms. The previously proposed transport models all have limits to their application; a unified model of charge carrier transport in organic semiconductors is still lacking. This thesis will focus on the effect of temperature on transport mechanisms in amorphous semiconductors, studying the impact of molecular relaxations on electronic properties, and proposing an approach (combining the MN behavior study and AC measurement analysis) which might be useful for clarifying charge carrier transport mechanisms in other glassy organic polymers.

1.3 Objectives

There are two main types of organic semiconducting materials: small molecules and polymers. Among conjugated polymers, Poly(3-hexylthiophene-2,5-diyl) (P3HT), a polythiophene derivative, is widely used in organic electronics as a representative p-type material due to its high charge carrier mobility and good air stability. P3HT can form head-tail head-tail (HT-HT) regioregular structures, self-organized into lamellar sheets, as shown in Figure 1-3.[4, 5] The regular end-to-end arrangement of its side chains ensure an efficient π-π stacking of the polymer backbone.[17] With the increase of the regioregularity, out-of-plane twists along the polymer backbones can be avoided. [4, 5] These characteristics make possible high charge carrier mobility of P3HT in the range of 10^{-5} to 10^{-1} cm^2/Vs.[18-20] However, the torsional motion of the thiophene rings in the main chain and the relaxation of hexyl side chain induce complexity to charge carrier transport in P3HT.[21, 22]

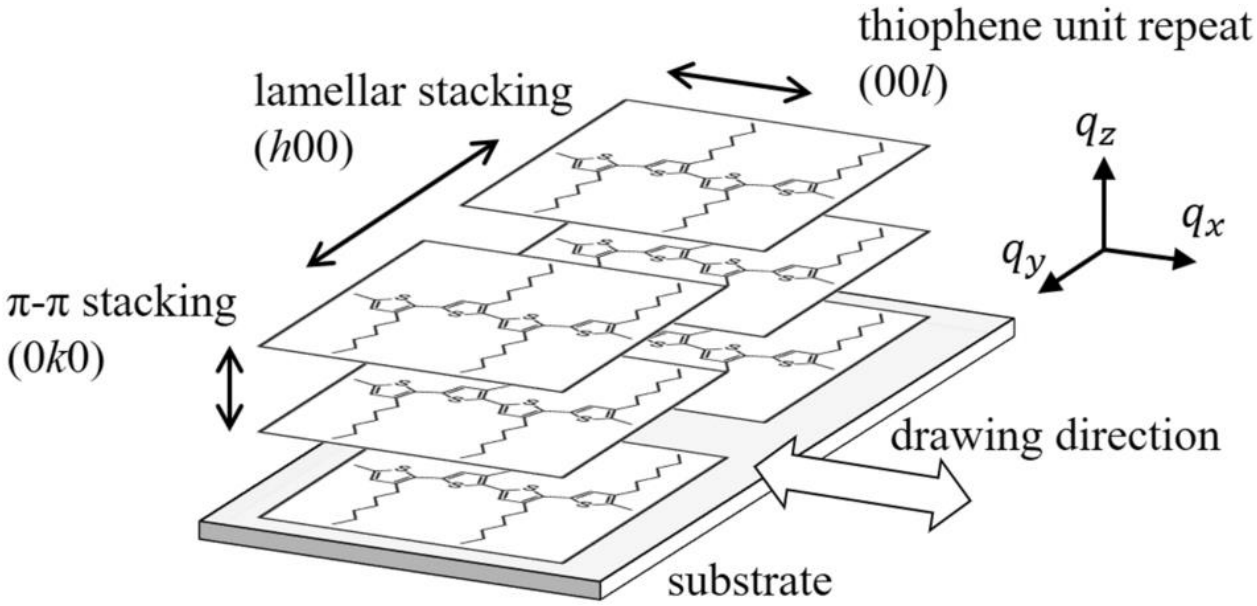

Figure 1-1 System schematic of molecular arrangement in ordered P3HT thin film. Reprinted from with permission from Ref. [23].

Among small molecule semiconducting materials, one distinctive example is a soluble fullerene derivative, namely n-type phenyl-C61-butyric acid methyl ester (PCBM). [24-26] PCBM has lower lowest unoccupied molecular orbital (LUMO) level compared to fullerene (C60), enabling easier electron injection processes with respect to C60.[27, 28] PCBM can undergo up to six reversible electron transfer processes due to its triply degenerate LUMO.[25, 29] Previous studies were focused on P3HT:PCBM blends, less attention was paid to the pure material.[30]

The objectives of this thesis are to:

(1) Study the charge carrier transport in P3HT and clarify the effect of glass transitions on its transport properties in glassy P3HT. Previous research was focused on its semi-crystalline form,[31-35] less attention was paid to the glassy polymer.

(2) Maximize the performance of elusive n-type semiconductor PCBM, study the charge carrier transport and illustrate the influence of temperature on its transport properties.

1.4 Outline of the thesis

In the following part of Chapter 1 we discuss previously proposed charge carrier transport models in organic semiconductors, such as band-like transport, variable range hopping, multiple trap and release model and percolation theory. We also discuss relaxation phenomena and other parameters which have effects on charge carrier transport in organic semiconductors. In Chapter 2 we introduce the Meyer Neldel rule and its microscopic origin (multi excitation entropy (MEE) model). In Chapter 3, we introduce working principles, injection processes and figures of merit in OFETs and present a method for measuring the activation energy. Chapter 4 is devoted to the description of experimental methods and characterization techniques employed in this thesis. Chapter 5 treats charge carrier transport mechanisms of dc and ac conduction in Poly(3-hexylthiophene-2,5-diyl) (P3HT). Chapter 6 is dedicated to charge carrier transport in a small molecule organic semiconductor PCBM. Chapter 7 general discussion and perspectives and Chapter 8 conclusions.

1.5 Proposed charge carrier transport models in organic semiconductors

1.5.1 Variable range hopping

Variable range hopping model is based on Marcus's semi-classical electron transfer theory and is described by Mott's Law. This model is widely used in the disordered systems to interpret the temperature dependence of charge carrier transport, i.e. the conductivity is proportional to $T^{\frac{1}{4}}$, as follows:

$$\sigma \propto T^{\frac{1}{4}} \quad (1\text{-}1)$$

Equation (1-1) is the Mott's law.[36-38]

And the average hopping distance is

$$< r > \propto T^{-\frac{1}{4}} \quad (1\text{-}2)$$

The hopping distance increases as the T decreases, this is why the model is called variable range hopping. Mott's variable range hopping model has been used in organic semiconductors to illustrate the charge carrier transport mechanism.[39-41]

The limits of the Mott's law are the following ones: (i) the localization radius of the charge carriers cannot be too small, the charge carrier hopping will only happen between nearest neighboring sites if the charge carriers are too localized; (ii) it only applies at low temperatures; (iii) the system needs to be highly disordered, while conjugated polymers feature ordered aggregates. The assumption of a constant density of states near the Fermi level always leads to the natural mismatch of the experimental data with the theory.[42]

1.5.2 Percolation

Since organic semiconductors are usually inhomogeneously disordered, charge transport could also locate in the sub percolation limit such that charge transport would be limited by the connectivity of conducting domains (while the poorly connected disordered domains would act as energy barriers ΔE and give the temperature dependence of the conductivity as $e^{-\Delta E/k_B T}$).[43] All in all, the conductivity is dominated by transport within and between ordered domains. Such a percolation mechanism for charge transport is thought to be consistent with recent microstructure studies. For instance, in Ref. [31] it is shown that transport occurs through aggregates (connected ordered regions) within an inhomogeneous disordered sample; in Ref. [44], it is shown that the mobility of the field-effect transistors could be increased dramatically by a small increase of the volume fraction of aggregates.

1.5.3 Band-like transport

In the absence of physical and chemical defects, charge carrier transport in organic semiconductors with a simple single-crystalline structure is determined by the interplay between electron-phonon couplings and intermolecular electronic couplings:[45] when electron-phonon couplings are weak, charge carriers are delocalized and behave as described in the band theory. This theory states that the energy spectrum of an electron moving in a periodic potential is constituted by conduction band and valence band. An electron with energy located within the conduction band will move like a free particle with an effective mass. Effects of the weak electron-phonon couplings to charge

transport can be taken into account by using a quasiparticle called polaron which describes electrons moving together with the dressed phonon cloud. The charge carrier mobility in this periodic potential generally decreases with increasing temperature due to the enhanced phonon scattering; When the electron-phonon couplings are stronger than the intermolecular electronic couplings, the charge carriers are completely localized on individual molecules and transported by hopping from one molecule to another. In such a region, the band-like theory cannot be applied anymore. Hopping transport is temperature-activated since the thermal fluctuations provide the activation energy for the charge carriers to overcome the energy barrier.

1.5.4 Multiple trap and release model

In some organic semiconductors, transport is limited by trap states induced by defects and impurities. These trap states are highly localized and carriers trapped in these states cannot escape easily from these locations. Charge carriers arriving at the trap site are captured instantaneously and with a large probability. And the release of the trapped carriers is temperature-activated. The effective mobility can be defined as[46, 47]

$$\mu_{eff} = \mu_0 \rho_0 e^{-\frac{E_T - E_C}{k_B T}} \quad (1\text{-}3)$$

where μ_0 is the band transport mobility, ρ_0 is the trap density, E_T is the energy of the trap depth and E_C is the energy of the conduction band edge. In real systems, the trap density will show an energy dependence. Here, by assuming an exponential distribution, one can arrive at an expression of the effective mobility as

$$\mu_{eff} = (1 + \frac{T}{T_c})[\frac{C(V - V_0)}{qN_T}]^{\frac{T_c}{T} - 2}\mu_0 \quad (1\text{-}4)$$

with T_c being the characteristic temperature of the assumed trap density distribution, C is the capacitance, and N_T is the effective density of states for the trap sites.

It is noted that the MTR model is applicable for systems that still have well-defined band structures with trap levels located within the bandgap. The most crucial parameter here that affects the charge transport is the trap energy E_T. Since the relaxation time of a trapped carrier is proportional to $e^{E_T/k_B T}$, more considerable trap energy may result in a more severe decrease in the mobility. This observation has been used to interpret results in Ref. [48-50].

1.5.5 Proposed unified model of charge carrier transport in organic semiconducting polymers

Researchers tried to develop a unified and widely applicable model of charge transport in semiconducting polymers. For instance, Noriega et al. studied samples of semicrystalline P3HT which were prepared at varying degrees of order.[31] They explained how the degree of disorder and (ordered) aggregation would influence charge transport, and why poorly ordered polymers could have high performance. First, they argued that the ordered regions are largely responsible for charge transport. This argument is based on the observation that charges must overcome an energy barrier to move from ordered regions to amorphous regions and charge carriers would stay in the ordered region (using P3HT model semicrystalline conjugated polymer where ordered and amorphous regions coexist to demonstrate this hypothesis). They studied charge transport in ordered regions by using a simple one dimensional tight-binding model. This model assumes hopping integrals are induced by energetic disordered local on-site hopping and nearest neighbor transport. They propose that the density of states of the aggregate in typical conjugated polymers is determined by the amount of paracrystallinity (measures the fluctuation of lattice space in the π-stacks) and seldom affected by on-site disorder. Further, the wave function in the tail of density of states represents localized states that can act as traps for the delocalized band states.

Then, they investigate the collected experimental data to prove the impact of paracrystallinity on charge transport properties. They divide the conjugated polymers into two categories. In one category, they have the totally amorphous materials. These materials lack any long-range order and their X-ray scattering halo are characterized by featureless and broad signals. Charge carrier transport in these materials is limited by hopping between localized states in a broad density of states. In the second class, they have materials which can form inter-connected aggregates either of long-range or short-range type. For the long-range ordered type, referred as "classical semicrystalline", their transport can be explained by the trapping-limited picture where the greater is the disorder, the deeper is the trap and the larger is the activation energy. For the short-range type, they argued that, since the mean free path in the π-stack is smaller than the aggregate length, the paracrystallinity-dominated mechanism still applies; with a comparable activation energy as semicrystalline materials, this type can achieve high charge transport performance.

Finally, by bringing together the discussions, they propose that short-range ordered aggregations in high MW polymers are enough for long-range charge transport and it explains why sometimes poor ordered polymers have higher performance. We will show below in Chapter 6 that in mostly amorphous thin film, hopping in amorphous region instead of the ordered region would dominate the charge transport and provide an explanation for the phenomenon of increased crystallinity leading to lower mobility.

1.6 Relaxation phenomena in organic materials

1.6.1 Relaxation and its characterizations

When a system experiences an external change of the stimuli such as electric field or temperature, it will be in a non-equilibrium state. The system will then relax. In conjugated polymers, after temperature or electric field changes, molecular relaxations are observable. Such relaxations can be due to a variety of movements of molecular segments or additives/impurities.[51]

With increasing of the temperature, the state of semiconducting polymers may change in the sequence: solid state, with mixture of amorphous and crystalline region; glassy state, characterized by non-equilibrium and non-crystalline amorphous structure; rubbery state, which leads to softness and flexibility; and viscous fluid state. In some polymers, e.g. cross-linked resins, there is no rubbery state and viscous fluid state.

There are typically three relaxation processes, called γ, β and α, in the glassy state. They can be observed by plotting the modulus of the polymer (the ratio of stress to the elastic strain) versus temperature, as shown in Figure 1-3.

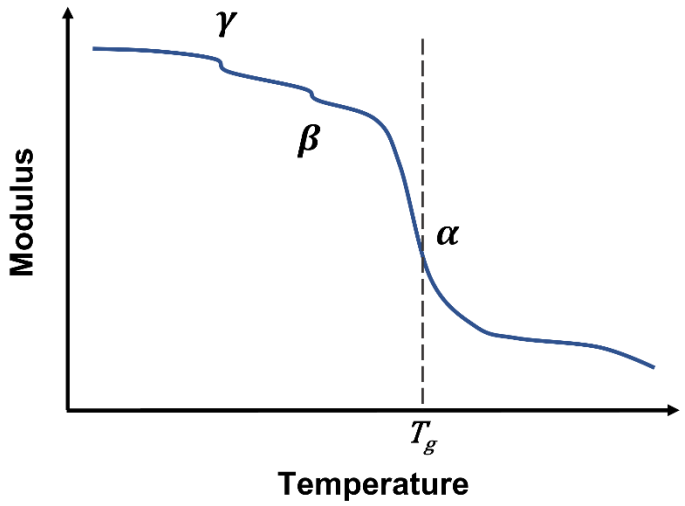

Figure 1-2 Illustration of temperature dependence of the modulus of the polymer.

The motions corresponding to the gamma and beta relaxations are illustrated in Figure 1-3. The γ relaxation corresponds to the side chain movement, this movement might be the vibration of the side chain or rotation of the side chain if it contains polar bonds. The β relaxation usually involves the movements of chain segments.

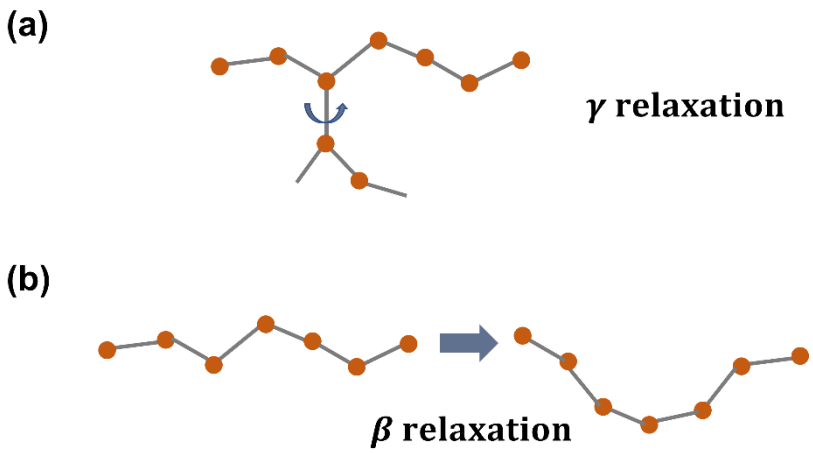

Figure 1-3 Two different local motions (a) γ relaxation, side group movement, and (b) β relaxation, chain segment movement.

Except from local motions, there is also the structural relaxation, α relaxation, which refers to the rearrangement and movement of the overall polymer chain. It usually happens when the amorphous polymer experiences a dramatic change in the modulus in the region of glass transition temperature.

The structural relaxation can be characterized by the following macroscopic features, which permits the observation of this transition:

(1) Change of enthalpy or entropy, can be detected by techniques such as Differential Scanning Calorimetry (DSC)

The heat capacity of the sample is measured using heat flow between the sample and reference, as a function of time. Initially, the sample is heated above the glass transition temperature (higher than T_g to remove the thermal history of the sample) and then cooled down to below T_g at a particular heating and cooling rate. Afterwards, the sample is reheated with the same heating rate. The temperature at which the heat capacity exhibits a step change is the glass transition temperature. DSC requires a simple experimental setup, and it is suitable to identify the various thermal transitions in a wide temperature range. T_g of polymers can be measured easily using DSC except for polymers with T_g below ambient temperature, highly crosslinked polymers, polymers in single layer nanoscale film form and those with small capacity changes with respect to crystallization, during cooling. [52]

(2) The change of specific volume of a thin film, can be measured using techniques such as thermodilatometry

In thermodilatometry, the volume of a polymeric sample is measured as a function of temperature under isobaric conditions. A change in slope of the volume versus temperature curve corresponds to the glass transition region. This technique is mainly suitable for probing T_g in amorphous polymers. The main disadvantage of thermodilatometry is that it requires large amount of sample to extract the glass transition temperature [52, 53]

(3) The change of mechanical properties can be measured by techniques such as Dynamic Mechanical Analysis (DMA)

In dynamic mechanical analysis, an oscillatory strain (or stress) is applied to the material to obtain the mechanical response of the material with respect to the temperature and frequency. [53] Storage

modulus (E') and loss modulus (E'') are obtained from DMA measurements and the mechanical damping factor (tan δ) is calculated using storage and loss modulus. T_g is extracted from the tan δ curve. DMA is highly preferred to detect the glass temperature of crystalline conjugated polymers. The limitations of DMA are that it is difficult to determine T_g if the sample has multiple thermal transitions, and it that it can only be applied to bulk material.[52]

(4) Dielectric properties can be measured by techniques such as Dielectric Spectroscopy, Thermal Stimulated Depolarization (TSD) and Thermal Stimulated Current (TSC)

Dielectric spectroscopy is employed to study the dielectric response of the material subjected to a small magnitude electric field as a function of fixed or variable frequencies.[54] This technique can be used to measure the AC, DC conductivity and dielectric properties such as dielectric constant and dielectric loss of the material.[55] Various relaxations processes can be measured over the frequency range of from 10^{-6} to 10^{12} Hz, it can reveal a lot of information on the structure of the material. Dielectric spectroscopy is suitable to measure T_g of polymer bulk material as well as thin films. However, this technique is limited in measuring high conductivity materials, the low frequency conductivity slope will lead to the difficulties in analyzing dielectric relaxation response of the material.[52] TSD/C are also widely used to determine the glass transition temperature of the material. The sample is subjected to polarization with DC electric field and the polarization is maintained under cooling process. Afterwards, depolarization takes place during sample heating process and the depolarization current is measured. Depolarization current peak region is corresponding to the glass transition and the temperature at which the maximum intensity of the depolarization current is T_g. TSD/C technique is the suitable method to deduce T_g in wide range of materials such as amorphous and crystalline polymers, and organic glass formers. It will be difficult to use TSD/C measurement if the sample contains mobile ions. [53]

The relaxations will also have a strong influence on the conductivity of organic semiconductors. It was found that when α relaxation happens, instead of following the Arrhenius Law, the relaxation frequency of the substance would follow the Williams-Landel-Ferry (WLF) equation [56]

$$ln\left(\frac{\omega}{\omega_g}\right) = A\frac{T-T_g}{B+T-T_g}, \quad (1\text{-}5)$$

where T_g is the glass transition temperature, ω is the relaxation frequency, ω_g is the relaxation frequency at glass transition temperature and A, B are constants.

However, all of those methods will only work on the determination of the glass transition temperature and the change of conductivity or dielectric properties of the material, the illustration of the detailed charge carrier transport process is still missing. In the following chapter, we will introduce a theory which has been well established in many physical processes. The charge carrier transport processes in P3HT will be explained unambiguously by studying this theory in the DC conditions and performing the measurement of the same sample in AC conditions.

1.6.2 The effect of relaxations on charge carrier transport

Most previous work on charge carrier transport in organic semiconductors have focused on semi-crystalline material and did not discuss the effect of glass transitions in organic semiconductors on transport measurements.[31-35] Some of them observed that the relaxations would influence transport: for instance, Obrzut, et. al. studied semi-crystalline P3HT from 193 K to 333K (they see no sign of the glass transition in their measurements), and they have measured DC, AC conductivity and dielectric response normal to the plane of a P3HT film, with 40-50 μm between electrodes, in a capacitor geometry. As shown in Figure 1-3, they find that the relaxation of the side group, the γ relaxation, causes scattering of carriers moving on the molecular backbone, which leads to the decrease of the device performance.[57] Such effects are indeed well established, and different from what we report in this thesis. We find that charge carriers in glassy material must hop from one molecule to another for DC current to traverse the interelectrode distance. The experimental observation of the positive effect of relaxation on charge carrier mobilities has been reported in a few publications. [58, 59] However, these have either emphasized device performance or the effect of scattering at high temperatures. For instance, Shen et. al. reported the charge carrier mobility of P3HT went faster from ca. 385 to 415 K (the region right after the linear plot and before the

scattering effect), shown in Figure 1-3. [59] As we discuss later in this thesis, this positive effect of the relaxations is also important and is much greater than the scattering effect.

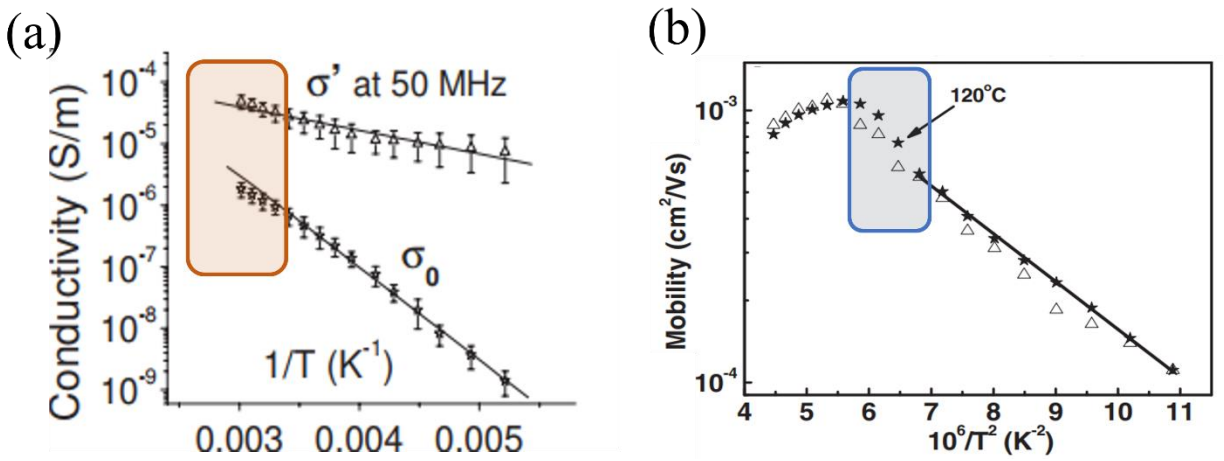

Figure 1-4 The dependence of (a) conductivity and (b) charge carrier mobility on temperature, reprinted with permission from Ref. [57] and [59].

1.7 Other effects which influence the charge carrier transport process

The stability of the organic materials is a common issue in the development of organic electronics. The degradation of the devices and formation of new defects due to the exposure to the external conditions will result in the decrease of the charge carrier mobility. [60, 61] Khelifi et al. studied the charge carrier transport in P3HT and PCBM blender through the admittance spectroscopy and capacitance voltage measurements under various temperatures. [61] The samples were measured with and without encapsulation. Their admittance spectroscopy measurements show two defect states with activation energies of 53 and 100 meV and the defect concentration is 10 times higher in the samples without encapsulation. Those defects were attributed to the charge transfer complex formed between O_2 and P3HT and they would lead to the decrease of charge carrier mobility. [60, 61]

To avoid the effect of oxygen, we prepared our samples in the nitrogen filled glovebox and measured it in a vacuum probe station which is connected to the glovebox.

The polarization at the interface or inside the organic material will also have some impact in the charge carrier transport process. For instance, Uludag et al. studied the dielectric properties of P3HT/CSA composites, they found that the real part of the complex permittivity decreased with the frequency increased from 20 to 10^7 Hz.[62] They attributed this behavior to the Maxwell-Wagner-Sillars interfacial polarization mechanism (MWS polarization may occur either at the inner dielectric boundaries or at the interface of electrode and dielectric). They propose that the dielectric material can be treated as the well conducting region, e.g. grains, surrounded by the poorly conducting region, e.g. grain boundaries. At low frequencies, the charge carriers will move to the grain boundaries, the accumulation of electrons at the boundaries will lead to a high-order polarization which manifests itself as high dielectric constant. We will show in Chapter 5 that it is not the case here, in the mostly amorphous material, the poorly conducting region is distributed large scale and randomly in the film, the ac conductivity increases with frequency.

Researchers report that the room temperature molecular motions also influence the charge carrier transport process. Troisi et al. studied the charge carrier transport in crystalline organic semiconductors.[63] They employed a one dimensional stack of planar conjugated molecules with one molecular orbital per molecules to calculate the charge carrier mobility under different temperatures. They took pentacene as an example, the initial nuclear positions are randomly selected from the Boltzmann distribution of non interacting harmonic oscillators. The displacement of the molecules is calculated from the Gaussian distribution. The temperature dependence of charge carrier mobility is determined from Einstein relation. They suggest that the charge carrier transport process in crystalline organic semiconductors at room temperature is neither polaronic nor the mixture of thermally activated hopping and polaronic transport. The room temperature molecular motions in organic crystals are adequate to destroy the translational symmetry of the electronic Hamiltonian, and thereby localize the charge carriers, it makes the band like transport theory insufficient for room temperature organic cystals. However, in the disordered organic semiconductors with high activation energies, the case is very different. The hopping process is not

fully free and random, and the potential well is not shallow enough for the Einstein relation and Gaussian distribution to be applicable.

CHAPTER 2 LITERATURE REVIEW: THE MEYER NELDEL RULE AND ITS MICROSCOPIC ORIGIN: MULTI EXCITATION ENTROPY MODEL

2.1 Introduction

The common factor among various charge carrier transport models in semiconductors is the existence of an activation energy. It has been well established that various physical processes, including charge carrier transport in semiconductors are temperature activated and follow the Arrhenius law: [64]

$$X = X_0 e^{-\Delta E/k_B T} \qquad (2\text{-}1)$$

where X is an observable such as the mobility μ, X_0 is the activation prefactor, ΔE is the activation energy, k_B is the Boltzmann constant, and T is the temperature. Since the 1920s, it has been found experimentally, even though the underlying mechanisms were not always clear, that for a related group of processes which are temperature activated, the prefactor obeys the relation: [65]

$$X_0 = X_{00} e^{\Delta E/k_B T_{iso}} \qquad (2\text{-}2)$$

which leads to

$$ln\, X_0 = ln\, X_{00} + \frac{\Delta E}{k_B T_{iso}} \qquad (2\text{-}3)$$

where X_{00} is an activation prefactor and T_{iso} is called the isokinetic or Meyer Neldel temperature, since X becomes independent of ΔE when $T = T_{iso}$. Combining Equation (2-3) with Equation (2-1), we obtain

$$ln\, X = ln\, X_{00} + \frac{\Delta E}{k_B T_{iso}} - \frac{\Delta E}{k_B T} \qquad (2\text{-}4)$$

Equation (2-4) is known as the Meyer-Neldel rule (MNR), since it was reported by Meyer and Neldel in describing the experimentally observed conductivity of disordered materials;[66] as the compensation law, because the exponential term $e^{\Delta E/k_B T_{iso}}$ in X_0 compensates the decreasing exponential, $e^{-\Delta E/k_B T}$, as ΔE is increased; and as the isokinetic law, since X becomes independent of ΔE when $T = T_{iso}$. [65]

The MNR can be represented by a plot of $\ln X$ versus the inverse temperature which is called Arrhenius plot: the lines depend on different Arrhenius parameters and will intersect at T_{iso}, as indicated in Figure 2-1.

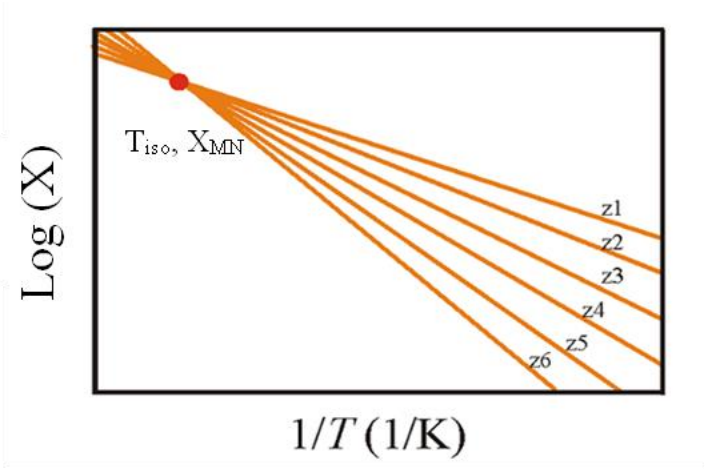

Figure 2-1 Observation of Meyer-Neldel rule: an observable (e.g. mobility or current) versus 1/T, where z is a variable parameter (e.g. gate voltage, V_g). Reprinted with permission from Ref. [67].

MNR has been observed in the transport properties of amorphous and crystalline silicon,[68-71] catalyzed chemical reactions,[72] solid state diffusion in crystals,[73] biological and geological substances.[74, 75]

2.2 MNR in organic semiconductors

In inorganic semiconductors, such as Si and Ge, in which the charge carrier mean free path is larger than the lattice constant, charge transport can be described by the band theory and the mobility has a power law dependence upon temperature $\ln \mu \propto T^{-n}$ with n=1-2. [76] However, band transport properties are rarely observed in organic semiconductors.

It has been found that the electron or hole mobility, μ, in many organic semiconductors,[6,19-22] including fullerene,[19] polythiophene,[20] pentacene,[6] and N-alkyl perylene diimides,[21] follow MNR. MNR was also observed in the ac conductivity of amorphous chalcogenides.[77]

For instance, MNR has been observed in disordered fullerene film-based devices fabricated using physical vapor deposition.[78] The schematic structure of the device is shown in Figure 2-2 (a). From

the Arrhenius plot, as depicted in Figure 2-2 (b), a crossing point of extrapolated data lines indicates the MNR behavior and permits to deduce the MN parameters. The isokinetic temperature obtained from OFETs based on C_{60} is $T_{iso} = 408K$, corresponding to a MN energy of $E_{MN} = 35\ meV$.

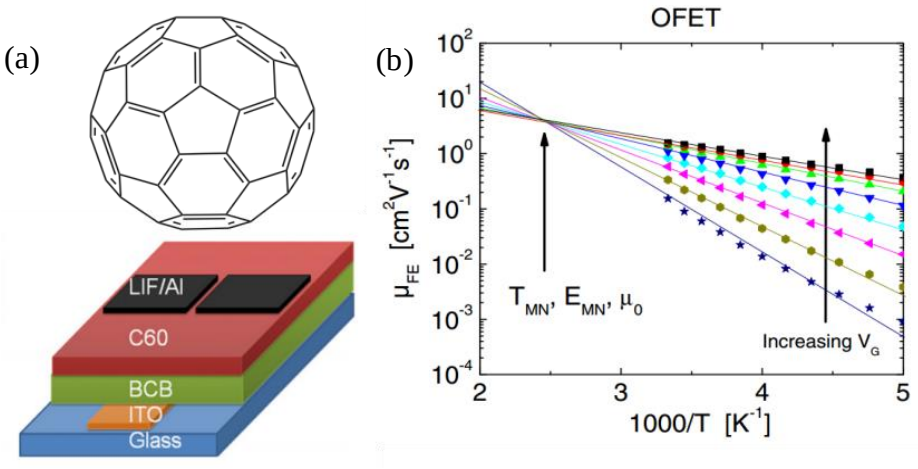

Figure 2-2 (a) System schematic of the OFET investigated and (b) observation of MNR in the OFET: Temperature dependence of μ at different V_g. Reprinted with permission from Ref. [78].

This MNR has also been observed in pentacene-based OFETs. Figure 2-3 shows temperature dependence of charge carrier mobility plotted at different V_g. MNR is observed to be at the point of T_{iso}=465 K.

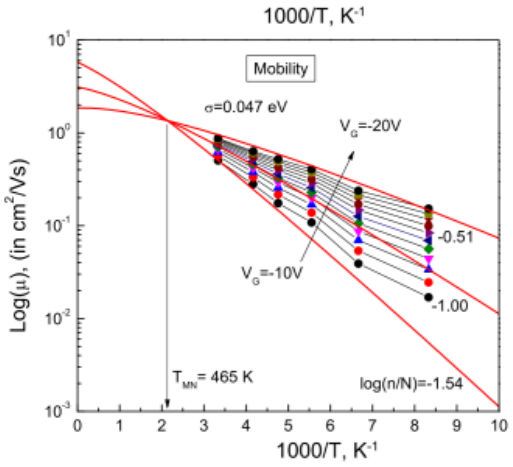

Figure 2-3 Temperature dependence of μ in pentacene films measured at different V_g. The T_{iso} is indicated in the figure. Reprinted with permission from Ref. [79].

In P3HT-based OFETs, a similar behavior is observed. As Figure 2-4 shows, the V_g dependence of charge carrier mobility disappears at the T_{iso}, which confirms the presence of MNR. However, the highest temperature studied here is ca. 300 K. It is of interest to study the effect of the temperature on charge carrier transport at higher temperatures.

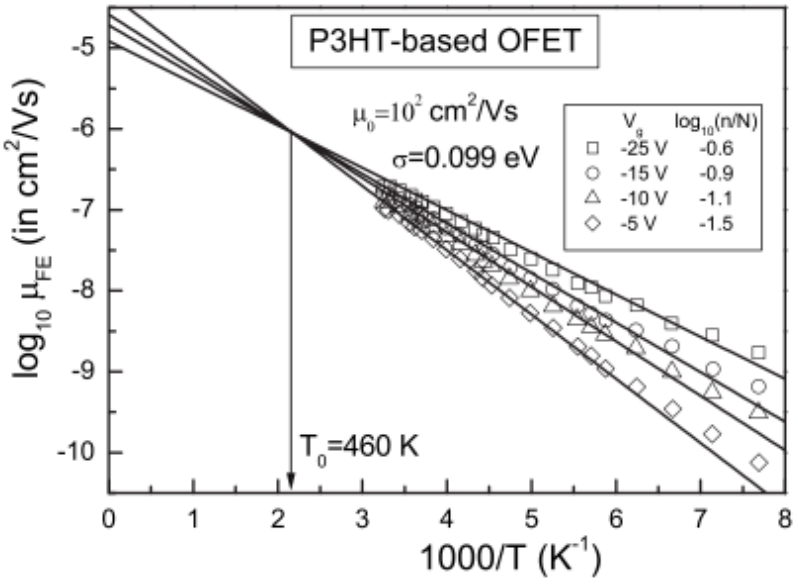

Figure 2-4 Temperature dependence of the μ in P3HT-based FETs measured at different V_g. Reprinted with permission from Ref. [80].

2.3 MEE model

In the 1980s, the MNR was explained by a number of authors,[65] including Linert[81] and Yelon and Movaghar[82] who called their version of the explanation the multi-excitation entropy (MEE) model. These explanations are based upon the key observation of the MEE model that, when the activation energy ΔE is much larger than both the energy of the available excitations and the thermal fluctuation energy, multiple excitations are necessary to obtain the energy to overcome the activation barrier. Thus, a contribution from the entropy of the collected excitations must be taken into account [65], and it leads to the MNR or compensation law. This idea can be explained by the

following simple examples. As depicted in Figure 2-5, suppose that we have an electron trapped in a potential well, and this electron can absorb the energy of a phonon to jump out of this potential well. According to the rule of statistical physics, the rate of this electron to jump out of the potential well should have an exponential dependence on the gap of this potential well and the temperature of underline system. The observable, e.g. mobility, current or conductivity, can be given as the Arrhenius law, as Equation 2-1 shows.

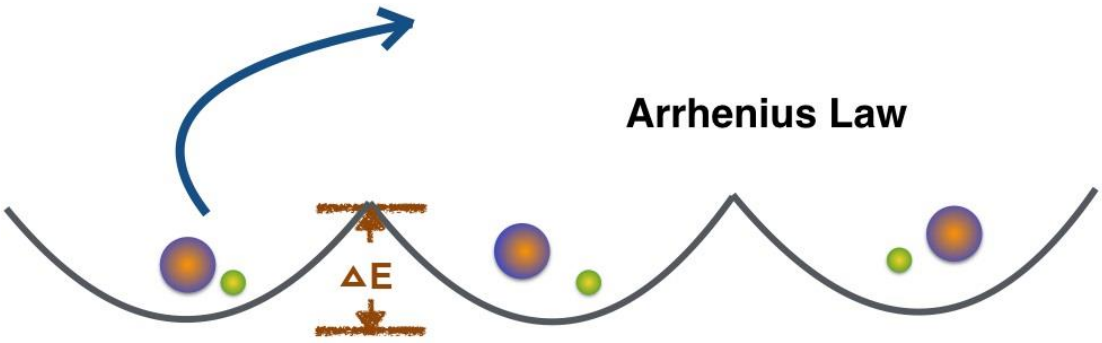

Figure 2-5 A simplified model to explain Arrhenius Law. The larger ball represents electron, the smaller one is the phonon, the arrow means the electron changed from trapped state to de-trapped state.

However, when the depth of the potential well is much larger than the phonon energy and thermal fluctuation, as depicted in Figure 2-6, multiple phonons must be collected by the electron to de-trap, i.e., a compensation from multi phonon entropy must be taken into account. For instance, if there are ten phonons available, and the electron just needs to absorb the energy of three phonons to jump out the potential well, then the entropy term S of the phonon should appear in the model.

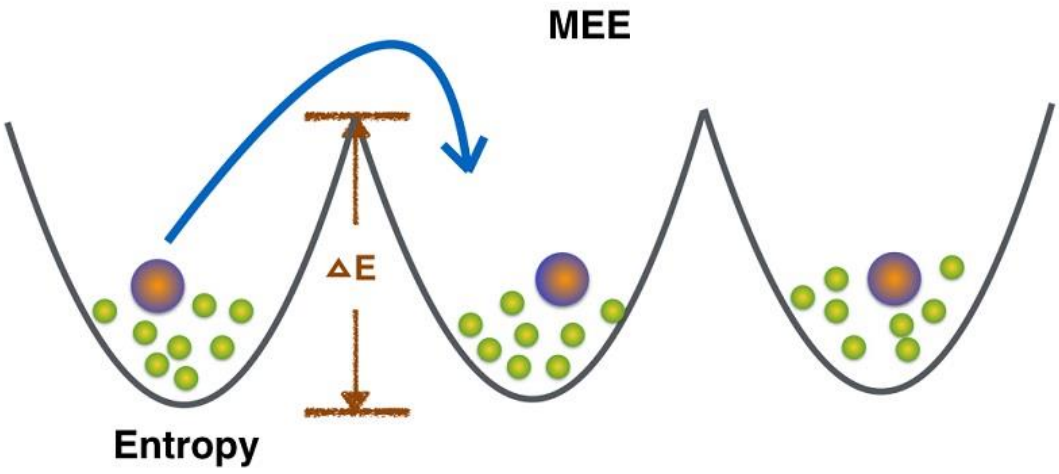

Figure 2-6 A simplified model when activation energy is large.

In the case of high temperature and strong coupling, we need to consider the entropy of the electron from the trapped state to detrapped state, so ΔS should include both the phonon and the electron parts. We need to treat the electron and phonon as one system, instead of separately.

It has been shown that the MN energy (MNE) appears to be given by

$$E_{MN} = k_B T_{iso} = \frac{\hbar \upsilon}{ln\, \kappa} \qquad (2\text{-}5)$$

In Equation (2-5), $\hbar \upsilon$ is the energy of the excitations, normally phonons in inorganic solids, and infrared or Raman vibrations in organic solids, and κ is a coupling constant between electrons and phonons. [65, 82, 83] This E_{MN} is extracted from a bath, whose source is the electron-phonon interaction. Semiconductors with similar structure will exhibit similar E_{MN}, since they obtain their excitation energy from similar thermal baths.[83] Equation (2-5) may provide important insights in the study of organic semiconductors. For example, it has recently been shown that the proton conductivity in perovskite-type metal oxides can be enhanced by tuning a lattice vibration frequency towards a desirable T_{iso}.[84] For some properties of some materials, described in Equation (2-4), such as conductivity in amorphous chalcogenides,[85] a correlation has been observed between X_{00} and T_{iso}. This has been explained by the dependence of the conductivity on κ, the electron-

phonon coupling, and the dependence of E_{MN} upon κ, expressed in Equation (2-5). [86] This may provide important insights in the study of semiconductors. For instance, a low T_{iso} corresponds to a large electron-phonon coupling constant in the chalcogenides and the material becomes less conducting as the polaronic interactions increase.[86] Thus, the correlation between X_{00} and T_{iso} can be used to identify the conduction mechanism. Polaronic conductors exhibit a positive correlation ($dX_{00}/dT_{iso} > 0$) while conductors featuring trap limited mechanism exhibit a negative correlation ($dX_{00}/dT_{iso} < 0$).[85]

The MEE model can be used as a general model to explain a large variety of experimental data [82, 87-89], while other methods [65] will generally require some sort of disorder and a Gaussian distribution of the density of states. However, MNR is usually observed in systems where the charge carriers are deeply trapped, while the material can be either disordered or crystalline. The MEE model has also been verified by molecular dynamics calculations of surface diffusion on metals which have large activation energies.[90, 91] As pointed out by Boisvert et al [90], the activation energy calculated by assuming an attempt frequency for jumps which is equal to the phonon frequency in surface diffusion at high temperature can lead to an error of the diffusion coefficient by a factor of 10. The recent atomistic simulations of Gelin, et. al. also confirms the entropic nature of the compensating term.[91] They find that the experimental compensation effect of diffusion process in silicon and aluminum crystals originates from the broadening vibrational spectra (i.e. lower and higher frequency phonons), typically in softening solids. This is associated with the entropy of the system which is proportional to the activation energy. They find that the anti-compensation effect would only be observed in solids having dense structure, and with rigid interactions. These atoms have little free space to move and the collision of the atoms will be involved in the activation, it will shift the vibrational spectrum to the one with unusual high frequencies localized modes.

Despite considerable evidence in its favor, the MEE model of MNR's origin is still frequently contested.[92] A frequently cited[80] alternative, in which entropy plays no part, is the Gaussian density of states model, which explicitly assumes that virtually every disordered material exhibits this particular distribution, and implicitly assumes that excitation (phonon or vibrational) energies are comparable to ΔE. The first of these is implausible, and the second is clearly incorrect, since MNR is observed only in materials which exhibit ΔE much greater than those energies. It has also been shown that their explanation is unrealistic for the MNR in liquid semiconductors.[93] Their model

has been demonstrated in various experiments that it leads to unreasonable values for the prefactors.[92] Further, it predicts that the isokinetic temperature is related to the width of the assumed Gaussian density of states. This is in contradiction with experiment:[92] the Arrhenius plots of well-ordered and disordered materials with small, but variable, ΔE cross at 1/T=0 (their "isokinetic temperature" is infinite).

CHAPTER 3 FIELD-EFFECT MOBILITY AND CHARGE CARRIER DENSITY IN FIELD-EFFECT TRANSISTORS MAKING USE OF ORGANIC DISORDERED SEMICONDUCTING THIN FILMS

3.1 Working principle of organic field-effect transistors

Transistors have been widely used in electronic circuits as the active parts, such as switches and amplifiers. Figure 3-1 indicates a typical transistor output curve (drain-source current I_d versus drain-source voltage V_d). As long V_g is larger than the threshold voltage, V_{th}, i.e. $V_g > V_{th}$, the thin film transistor channel becomes conductive. When V_d is applied, the charge carriers start to flow between source and drain electrodes. The majority of charge carriers in p-type semiconductors are positive holes whereas the electrons are the majority charge carriers in n-type semiconductors. Injection and extraction of the charge carriers in the semiconductor channel take place at the drain and source electrodes.

The arrangement of electrodes, organic semiconductors, and the gate dielectric result in different architectures of the OFETs. The most used device architectures are top gate top contact, top gate bottom contact, bottom gate top contact and bottom gate bottom contact. Figure 3-1 (a) shows a bottom gate bottom contact structure OFET, it contains a gate electrode, a dielectric, a drain electrode, a source electrode and the organic semiconducting thin film. The source electrode is connected to the ground, the charge carriers begin to accumulate at the interface in the thin film channel when V_g is applied.

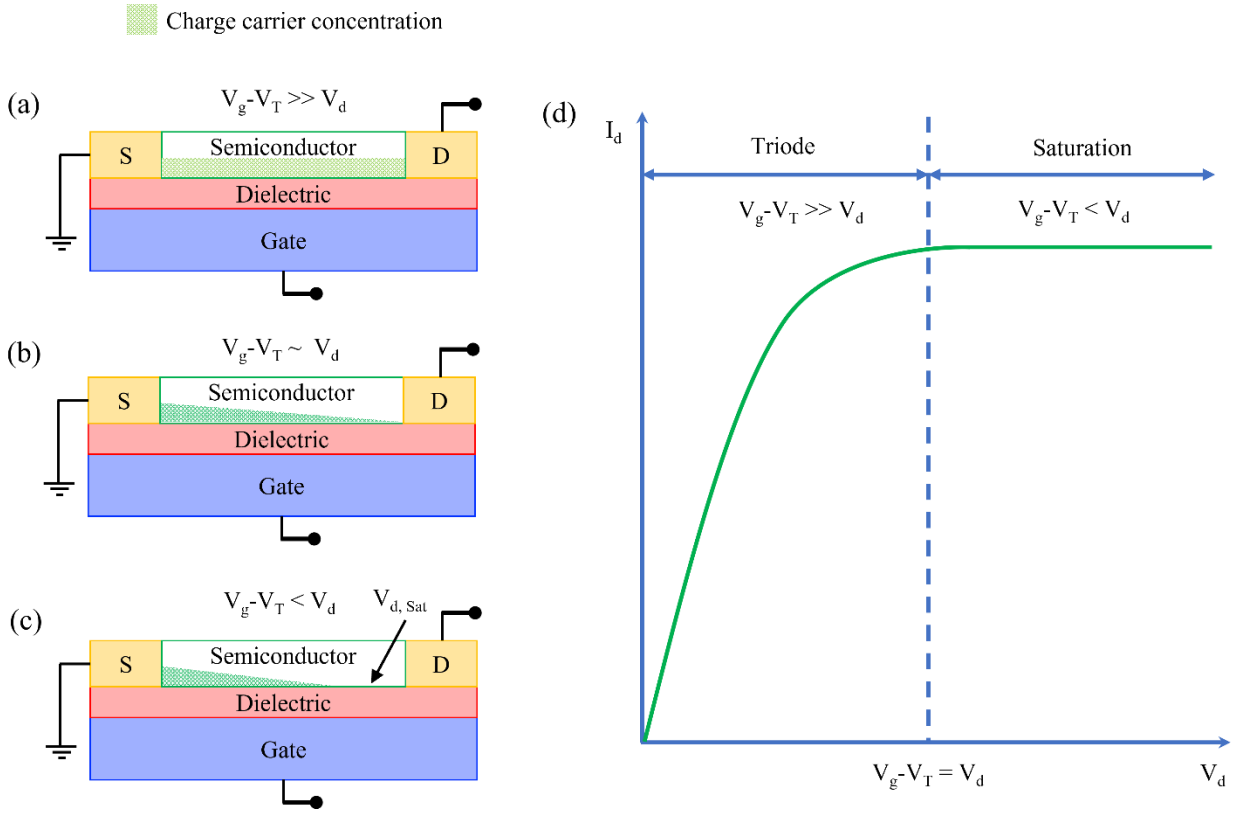

Figure 3-1 (a-c) Charge carrier concentration in bottom gate bottom contact OFETs under (a) linear region; (b) pinch-off region; (c) saturation region; (d) typical output curve of the transistor.

The device operation is explained with p-type (accumulation) organic semiconductor channel material and bottom gate bottom contact architecture in Figure 3-1 (a-c). As indicated in Figure 3-1 (a), when $V_d < V_g - V_{th}$, I_d will increase with the V_d, this is called linear region. When $V_d = V_g - V_{th}$, shown in Figure 3-1 (b), V_g is compensated by V_d and the thin film channel is pinched off at the drain electrode. A saturation region, Figure 3-1 (c), is reached at $V_d > V_g - V_{th}$ and I_d will not increase with V_d anymore due to the lack of majority charge carriers in the depletion region near the drain electrode. The current in the thin film is maintained by the charge carrier injected from the electrode.

The specific capacitance per unit area of the gate dielectric can be written as

$$C_i = \frac{\varepsilon k A}{d} \quad (3\text{-}1)$$

where ε is the vacuum permittivity, k is the dielectric constant, A is the area of the dielectric and d is the thickness of the dielectric layer.

At V_d=0, the charge carrier density can be written as

$$Q = C_i(V_g - V_{th}) \quad (3\text{-}2)$$

The charge carrier density will become a function of the distance from the source electrode when V_d increases, Equation (3-2) can then be written as

$$Q(x) = C_i\left(V_g - V_{th} - V(x)\right) \quad (3\text{-}3)$$

Then I_d can be written as

$$I_d = W\mu Q(x)E_x(x) \quad (3\text{-}4)$$

Where W is the channel width, μ the charge carrier mobility and $E_x(x) = \frac{dV(x)}{dx}$ the electric field applied in the x direction.

Combining Equation (3-3) and (3-4), we can obtain that in the linear region, i.e. $V_d << V_g$-V_{th}, [94]

$$I_d = \frac{WC_i}{L}\mu(V_g - V_{th} - \frac{V_d}{2})V_d \quad (3\text{-}5)$$

In the saturation region, $V_d = V_g$-V_{th}, I_d can be written as[94]

$$I_d = \frac{W\mu C_i}{2L}(V_g - V_{th})^2 \quad (3\text{-}6)$$

3.2 Field-effect mobility

The field effect mobility can then be derived from Equation (3-5) and (3-6). [64]

In the linear region, it is:

$$\mu_{lin} = \frac{L}{WCV_d}\frac{\partial I_d}{\partial V_g} \quad (3\text{-}7)$$

In the saturation region, it is:

$$\mu_{sat} = \frac{2L}{WC}\left(\frac{\partial\sqrt{I_{dsat}}}{\partial V_g}\right)^2 \quad (3\text{-}8)$$

3.3 Charge carrier density

The dc conductivity, σ_{dc}, is determined from

$$\sigma = L/(RWd) \qquad (3\text{-}9)$$

where R is the resistance (can be derived from the linear region of I_d versus V_d curve), d is the thickness of the thin film. The charge carrier density, n, can then be determined from

$$n = \sigma/(\mu e) \qquad (3\text{-}10)$$

where e is the elementary charge.[64]

3.4 Schottky barriers and charge carrier injection in OFETs

Charge carrier injection in OFETs depends on the work function of the source drain electrode and the position of the energy levels of the organic semiconductor. When the work function of the electrode is close to the highest occupied molecular orbital (HOMO) or LUMO levels, the charge carriers are more easily to be injected and contacts are called ohmic. The mismatch between the work function and the band edges is called the Schottky barrier. It will induce a contact resistance in the OFET.

3.5 Activation energy measurement in OFETs

In most studies of MN behavior, the activation energy is varied by preparing a number of samples in slightly different ways, e.g. changing the preparation conditions for samples with a specific composition, or by preparing closely related compositions.[65, 95] However, in studies of semiconductors, as is the case here, there is considerable advantage in preparing FETs, using the material under investigation as the semiconducting film transistor channel. Varying the gate-source voltage, V_g, modifies the band bending at the semiconductor dielectric interface. This changes the energy distribution of charge carriers near the dielectric, compared with those farther away, thus changing the activation energy, ΔE.

In classic transistor technology, based upon small gap, crystalline, inorganic semiconductors, the number of thermally activated charge carriers is large at moderate values of T, as is the charge carrier mobility, μ. As expected for band transport, it is not thermally activated.[96]

These conditions are not expected to apply to organic semiconductors. The charge carrier density is not strongly dependent upon T. In contrast, the charge carrier mobility, μ, may be activated. In accumulation, except at the lowest voltages, the charge carriers induced by the gate-source voltage determine the source-drain current (in absence of charge carrier injection energy barriers). The activation energy ΔE is then controlled by V_g. Of course, the device must be functional over a wide enough temperature range for meaningful kinetics to be measured.

CHAPTER 4 EXPERIMENTAL METHODS AND TECHNIQUES

4.1 Microfabrication of Au electrode

The detailed procedure of microfabrication of conventional Au electrode is shown in Figure 4-1.

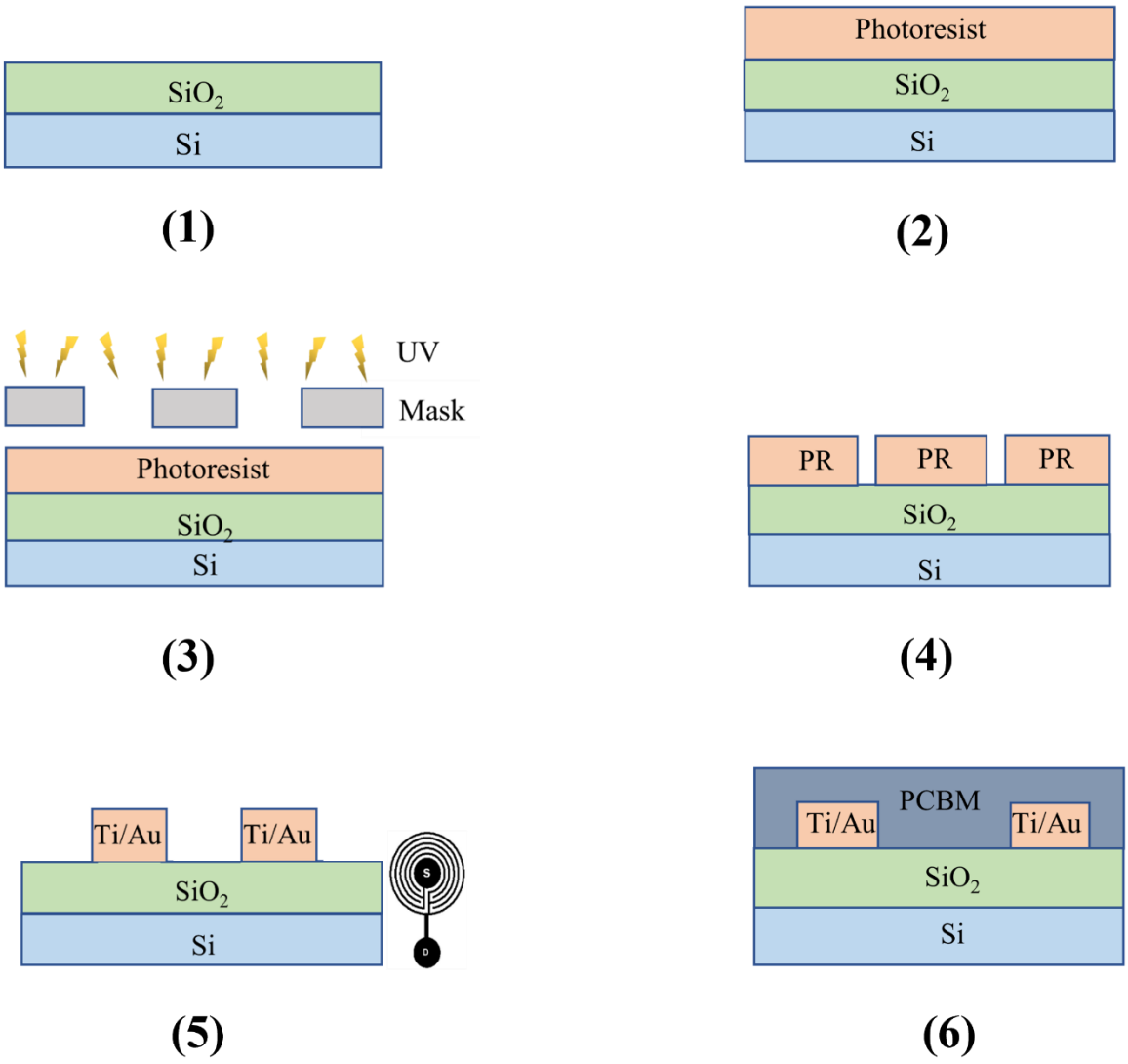

Figure 4-1 Microfabrication of Au electrodes by photolithography.

The initial substrate is a 200±10 nm-thick SiO_2 on 525±25 μm-thick silicon wafer purchased from WaferPro, San Jose, California. The heated substrate surface was exposed to hexamethyldisilazane (HMDS) gas to promote the adhesion of the photoresist using a Four YES oven. Then the

photoresist was deposited by spin coating at 4000 rpm for 30 s (thickness of ca. 1.56 µm). After the deposition, a soft-bake at 110 °C for 50 s was performed. The ultraviolet-ozone exposure was then operated at 7.7 mW by SUSS MicroTec HG Lamp; an energy density between 55 and 60 mJ/cm^2 was provided for ca. 7 s. The pattern was made by means of SUSS MicroTec Mask Aligner MA6/MB6. The photoresist development was made by soaking the substrate in the developer, stirring it for 1 min. The substrate was then washed by de-ionized water. The concentric regular geometry of the metallic Ti/Au (5/40 nm/nm) electrodes were evaporated by an electron beam evaporator. In Chapter 5, the channel of the devices has a width (W) of 2.5 cm and length (L) of 10 µm. In Chapter 6, the channel of the devices has a W of 1,500 μm and L of 20 µm. Then the substrates were immersed in the PG remover overnight to remove the residual resist. The patterned substrates were cleaned with a sequential ultrasonic bath in isopropanol alcohol (IPA), acetone and IPA, followed by UV exposure. Afterwards, the organic semiconductor, e.g. PCBM, was spin coated on the substrate.

4.2 Microfabrication of SWCNT/Au electrodes

Single-wall carbon nanotube (SWCNT) powder (purchased from RAYMOR NanoIntegris) was sequentially purified using 3M HNO3, 3M NaOH, and HCl. The SWCNTs were rinsed six times with de-ionized (DI) water to achieve a neutral final solution (pH ~ 7.8, as indicated by the pH/conductivity meter) and collected by the Polytetrafluoroethylene (PTFE) membrane filter. The SWCNT solution was prepared with the same method as previously reported by Cicoira et. al.[28] Briefly, 0.5% w/v sodium cholate and 5 mg SWCNT were dissolved in 400 mL of DI water and tip sonicated for 20 min. 4 ml of the solution were subsequently put in 80 ml of DI water, giving rise to a concentration of SWCNT ca. 6.25×10^{-4} mg/mL. The final solution was bath sonicated for another 30 min. The SWCNTs were then transferred to an amino cellulose membrane filter (0.22 µm Triton-Free MCE, purchased from Sigma Millipore) through vacuum filtration. The SWCNTs on the filter were then attached to a pre-cleaned SiO_2/Si substrate (i.e., sonication in DI water, IPA, Acetone, IPA, and UV ozone treatment) to make a SWCNT coating. The samples were immersed in a fresh acetone solution for 54 hours to dissolve the membrane. They were then placed inside a Type 21100 Tube Furnace for thermal annealing at 350 °C for 5 h in air to remove the solution

residue and improve the metal adhesion during electrode deposition. The substrate was then transferred to the clean room to perform the microfabrication (Figure 4-2). Circular Au/Ti electrodes (40 nm/5 nm) were photolithographically patterned on the SWCNT/SiO_2/Si substrate. To make a SWCNT-free channel within the interelectrode distance, samples were exposed to O_2 reactive ion etching (50 W RF power at 125 mTorr and 8 sccm etching rate), for 1 min.

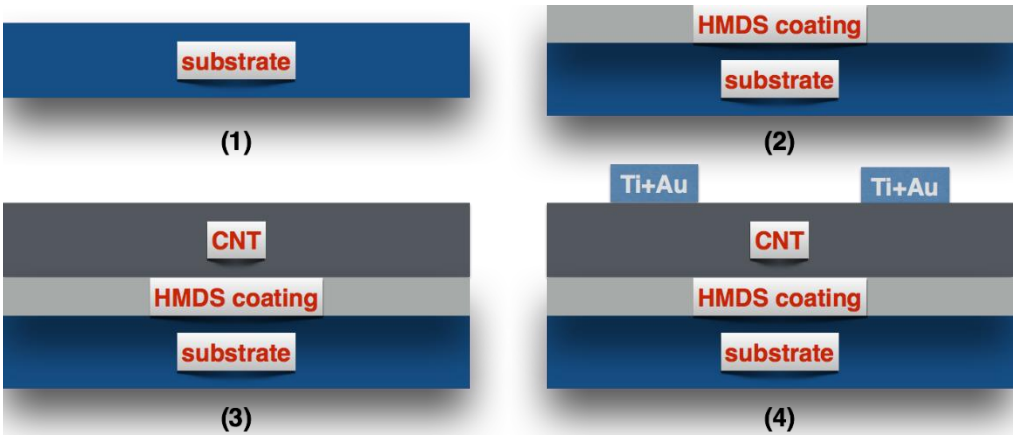

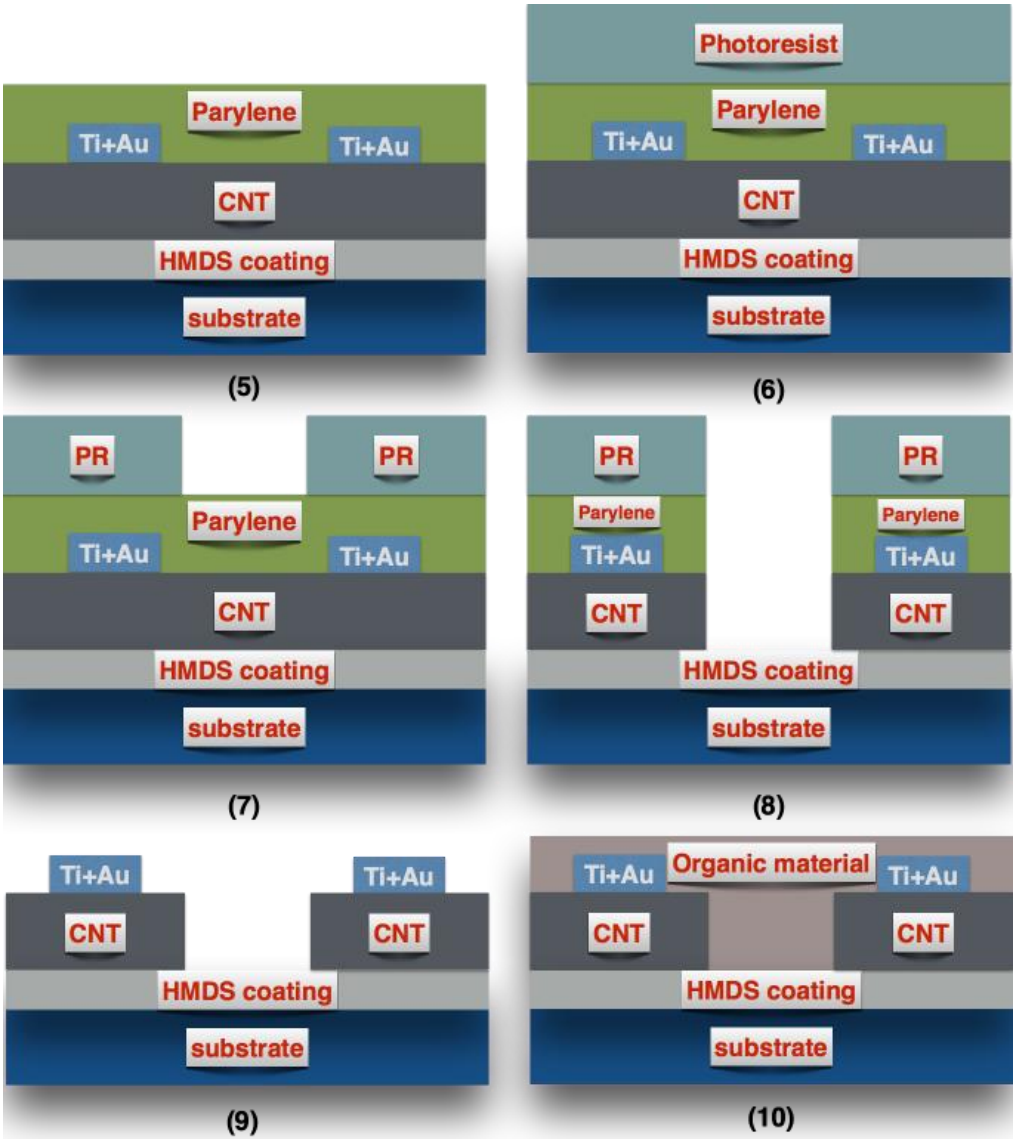

Figure 4-2 (1) Substrate: SiO_2 on doped Si; (2) HMDS-treated substrate; (3) SWCNT deposition; (4) metal electrode evaporation; (5) parylene coating; (6) photoresist coating; (7) developer; (8) etching; (9) parylene peel-off and 550 ℃ thermal treatment in vacuum for 1 h; (10) organic semiconducting film deposition (on substrates previously cleaned by low power sonication in acetone and IPA to remove the SWCNTs from the interelectrode region).

4.3 Thin film deposition

Thin films of RR P3HT (Solaris Chem Inc.) were deposited by spin coating (1,500 rpm, 100 s) from a (freshly prepared) 10 mgmL^{-1} solution in chlorobenzene under N_2 atmosphere, after the solution was stirred at 50 °C overnight. Each device was thermally treated on a hotplate at 110 °C for 10 min. The procedures are kept the same for all samples. Three molecular weights, ca. 20 kDa, 30-50 kDa, 80-90 kDa, are studied.

Thin films of PCBM (Solaris Chem Inc.) were spin coated (1500 rpm, 100 sec) from a 10 mg/mL solution in chlorobenzene under N_2 atmosphere. Prior to spin-coating, the solution was stirred overnight. Some of the devices were thermally treated on a hotplate at 50 °C for 2 h.

4.4 Techniques

4.4.1 Electrical characterization

Measurements of dc electrical properties were carried out using a semiconductor parameter analyzer Keithley 4200-SCS. During the measurements, the source electrode was connected to ground. Samples were measured in a micromanipulator cryogenic probe station with liquid nitrogen and copper heater to change the temperature. Measurements of ac electrical properties were performed using a Hewlett Packard 4192A LF impedance analyzer (5 Hz-13 MHz).

4.4.2 Structure and morphology film characterization

The surface topography of the samples was analyzed by atomic force microscopy (AFM) under ambient conditions, using a Digital Instruments Dimension 3100 (Santa Barbara, CA) equipped with a Nanoscope V controller (Bruker). The sample surface was scanned in tapping mode using an etched silicon cantilever (tip radius < 10 nm, spring constant ~ 40 N/m, and resonance frequency ~300 kHz) with a scan rate of 1 Hz. The height and phase AFM images were obtained with medium tip oscillation damping (20 % – 30 %).

The AFM images of (a) low MW P3HT, (b) medium MW P3HT, (c) high MW P3HT are shown in Figure 4-3. The value of the root mean square roughness (rms) is 1.6±0.1 nm for low MW,

5.3±0.6 nm for medium MW and 13.8±1.8 nm for high MW. Lower MW polymers are expected to be better dissolved, resulting in a lower surface roughness of the thin film.

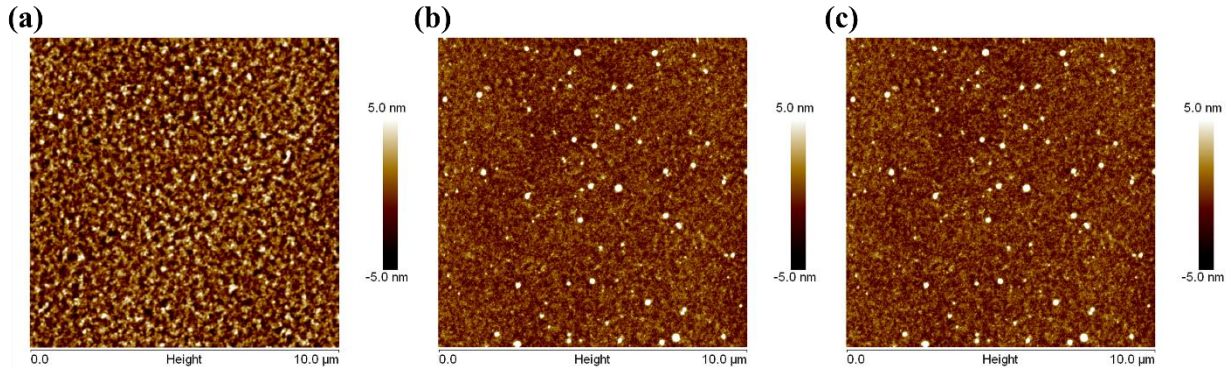

Figure 4-3 10 µm×10 µm-sized AFM images of (a) low MW P3HT, (b) medium MW P3HT, (c) high MW P3HT.

The electrodes with SWCNT were investigated by scanning electron microscopy (SEM). The surface of the samples is scanned by the electron beam. As compared to the optical microscope, electron microscope provides a higher magnification image with the utilization of electron gun. There are two different types of electrons are emitted from the sample after it is interacted with the incident electron beam, namely (i) secondary electron and (ii) backscattered electron (BSE). The secondary electrons are emitted due to the elastic interaction whereas the backscattered electrons are emitted due to the inelastic scattering. The surface feature and atomic number of the samples were analyzed using the secondary electrons and the BSE, respectively.[97, 98] SEM measurements in this thesis were carried out at an accelerating voltage of 5 kV in BSE and secondary electron imaging mode using the machine JEOL FEG-SEM.

X-ray diffraction (XRD) spectra of the thin films were scanned by a Bruker D8 diffractometer machine with the 1.54 Å wavelength (CuKa). The samples were scanned every $2\theta = 0.01$ with a time interval at 0.6 s. XRD can provide the orientation and structural information of the crystalline materials.[99, 100] It is based on the Bragg's law: $2dsin\theta = n\lambda$, where d is the interplanar spacing of the crystals, θ the angle of incidence, n an integral, and λ the wavelength. The diffraction will take place when conditions satisfy Bragg's law.[99, 101] The incidence monochromatic beam of X-rays will

be diffracted by the atoms of the materials to produce the diffraction peak, the peak intensity will be determined by the atoms within the lattice.[99]

4.4.3 Thickness characterization

The thickness of the organic semiconducting thin film was measured using a Dektak 150 Profilometer, a stylus profilometry based technique. The film thickness was 51.7±0.7 nm for low MW P3HT, 42.1±4.0 nm for medium MW, and 65.0±4.7 nm for high MW P3HT. The thickness of PCBM thin film was ca. 68.2±5.6 nm.

CHAPTER 5 ARTICLE 1: DEPENDENCE OF CHARGE CARRIER TRANSPORT ON MOLECULAR RELAXATIONS IN GLASSY POLY(3-HEXYLTHIOPHENE-2,5-DIYL) (P3HT)

5.1 Author and coauthors

Zhaojing Gao,[a] Manuel Reali,[a] Arthur Yelon*[a] and Clara Santato*[a]

a. Polytechnique Montreal, Engineering Physics Department, Montréal, Quebec, H3C 3A7, Canada

*Corresponding author: arthur.yelon@polymtl.ca; clara.santato@polymtl.ca.

Published on Materials Advances, 2022, DOI: 10.1039/D2MA00657J

5.2 Abstract

A positive effect of molecular relaxations, the movement of the molecular backbone and of chain segments on charge carrier transport processes in organic semiconductors, has not previously been reported. In this work, charge carrier transport mechanisms in amorphous glassy Poly(3-hexylthiophene-2,5-diyl) (P3HT) are determined unambiguously, both above and below the glass transition temperature, T_α. This is the result of measurements of temperature, electric field, and ac frequency dependence of charge carrier mobility and density in organic field effect transistors, based on regioregular P3HT of three different molecular weights. Relaxations play an important role in dc conductivity. At temperatures above T_α, under constant source-drain voltage, the hole-like polaronic carriers move with, and hop between, mobile polymer backbones. Below T_α, they hop between mobile chain segments of essentially immobile neighboring molecules. Under source-drain voltages at frequencies of 100 Hz and higher, charge carriers move on polymer backbones. This motion does not contribute to dc conductivity. These insights into the dependence of charge carrier transport properties upon the molecular properties should contribute to advances in stable organic photovoltaics, organic thermoelectrics, and thermally degradable electronics. The approach taken here should also be useful for clarifying conduction mechanisms in other polymeric semiconductors.

5.3 Introduction

Regio-regular Poly(3-hexylthiophene-2,5-diyl) (RR P3HT), whose monomer is shown in Figure 5-1, has been widely investigated for organic electronics, and the temperature dependence of μ has been shown to obey the Meyer-Neldel (MN) rule (MNR).[66, 102] Over the past two decades, improvements in P3HT film preparation have resulted in increased chemical purity, control of the molar mass and prolonged interchain conjugation. As a result, the μ of RR P3HT has improved considerably, from 10^{-5} to 10^{-1} cm^2/Vs.[18-20]

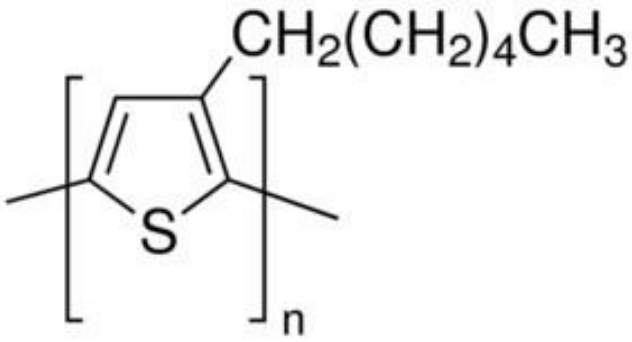

Figure 5-1 Repeating unit leading to P3HT.

Most previous work on charge carrier transport in P3HT has focused on semi-crystalline material and did not report the effect of glass transitions in glassy materials on transport.[31-35] It is essential to study the effect of molecular relaxations on transport. We optimized the device performance by appropriate technical choices: high boiling point solvent to obtain a uniform film morphology; adjustment of solution concentration to maximize the charge carrier mobility; surface treatment of dielectric SiO_2 with hexamethyldisilazane (HMDS) to decrease charge carrier trapping at the interface; choice of thermal treatment conditions to enlarge the device functional temperature range.

In this chapter, we measured the temperature, electric field and ac frequency dependence of μ in OFETs based on RR P3HT of three different molecular weights (MW), ca. 20, 30-50, 80-90 kDa, exhibiting different glass transition temperatures, T_α. The results are obtained both above and below the glass transition temperature.

5.4 Dependence of dc mobility, μ, on *T* under several V_g

The dependence of μ upon V_g and T for high MW RR P3HT is shown in Figure 5-2. Mobility increases with increasingly negative V_g. That is, the carriers are hole-like, as expected. At room temperature, its values range from 4×10^{-5} $cm^2V^{-1}s^{-1}$ to 3×10^{-4} $cm^2V^{-1}s^{-1}$, which is comparable with previous publications.[103, 104] As shown in Figure 5-2 (a), at $T < 290$ K, μ exhibits Arrhenius behavior for each V_g, and obeys, with a T_{iso} ca. 390 K. The activation energies are given in Table 5.1.

In Figure 5-2 (b), we observe that the slope of μ vs. *1/T* changes sharply at T=290 K, with μ becoming independent of V_g. This is not due to an annealing effect, which might modify the structure. If the measurement is repeated, the result is essentially the same. It is due to the transition between two conduction mechanisms, one dominant below 290 K, the other dominant above 300 K. The abrupt change in slope shown in Figure 5-2 (b) is typical of the α relaxation of glassy polymers, which has been investigated intensively.[56, 105] The α relaxation signifies that the thermally activated movement of the polymer backbones increases rapidly. This process becomes observable at the glass transition temperature, T_α. For RR P3HT of 80-90 kDa, T_α is reported to be 295 K.[105] This observation, and the observed temperature dependence discussed below, clearly show that the material investigated here is primarily in the glassy state, and that its dc conductivity is essentially that of the glass. We propose that the electric field acting on the charged sites causes the backbones to move, and that this process controls the mobility at $T > T_\alpha$. This produces a T_{iso} of 300 K. We propose that at $T < T_\alpha$, hopping of polaronic carriers is the controlling process. Details of this process will be developed, below in the discussion. We shall find, below, that hopping still takes place at $T \geq T_\alpha$. T_α is closely related to the MW, as indicated by the Flory-Fox equation, $T_\alpha = T_{\alpha,\infty} - \frac{K}{M_n}$, where $T_{\alpha,\infty}$ is T_α in the infinite MW limit and K is a specific constant for the material.[105, 106] As reported before, $T_{\alpha,\infty} = 22.1 \pm 1.2$ ℃, K $= 291 \pm 23$ kg/mol for Mw=80-90 kDa in RR P3HT; $T_{\alpha,\infty} = 2.9 \pm 0.2$ ℃, K $= 22 \pm 1$ kg/mol for Mw<20 kDa in RR P3HT. The resulting α transition temperature are $T_\alpha = 19$ ℃ for mw=80-90 kDa and $T_\alpha = 2$ ℃ for mw<20 kDa. [105]

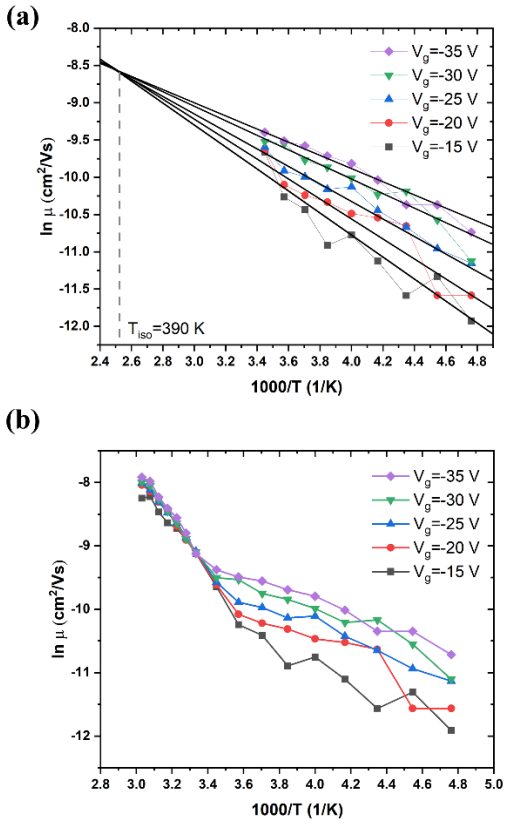

Figure 5-2 (a) Linear fitting results for high MW RR P3HT in the low T region, T=210-290 K. V_d=-20 V. (b) Dependence of mobility on T under different V_g in high MW RR P3HT. MW=80-90 kDa, V_d=-20 V, T=210-330 K, T_α=290 K.

Table 5.1 Activation energy of high MW RR P3HT, below T_α, as a function of V_g, V_d=-20 V.

V_g (V)	-15 V	-20 V	-25 V	-30 V	-35 V
E_a (meV) T=210-290 K	128	118	97	95	87

We also investigated RR P3HT, for low MW=ca. 20 kDa, with T_α near 275 K, and for medium MW=30-50 kDa, with T_α near 290 K. The dependence of μ on T under several V_g in low MW P3HT is shown in Figure 5-3. Behavior similar to that shown in Figure 5-2 is observed for low

MW P3HT. In the low T region, $T < T_\alpha$, μ depends upon V_g, and $ln\ \mu$ increases with T. In the high T region, $T > T_\alpha$, μ is independent of V_g with the slope increasing discontinuously, and then decreasing gradually. In this region, we see, more clearly than in Figure 5-2 (b), that μ does not obey Equation (2-1). The behavior of μ resembles that described in the empirical Williams-Landel-Ferry (WLF) equation, the signature of the α relaxation.[56] In what follows, we have determined the slopes of the Arrhenius plots, which we call the apparent values of ΔE. As shown in Figure 5-2 (b), taking V_g=-15 V as an example, the apparent ΔE changes from 406 meV at 290 K to 200 meV at 325 K.

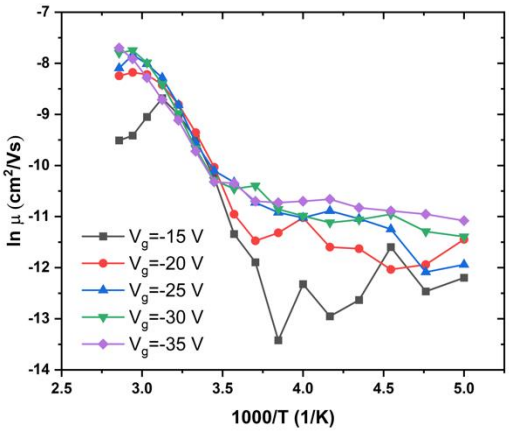

Figure 5-3 Dependence of μ on T under different V_g in low MW RR P3HT. MW<20 kDa, V_d=-15 V, T=200 to 350 K.

Unfortunately, the relation of μ to polymer relaxation puts limits to our ability to perform reproducible experiments and to obtain reliable device performance, near to, and above, T_α. We have verified that this is indeed the case for medium MW RR P3HT, MW=30-50 kDa. For this material, the behavior of a transistor was found to be quite different if high temperature measurements were performed immediately after low temperature measurements (Figure 5-4), or after 12 hours (Figure 5-5), during which it was left at room temperature. With relaxation times comparable to the time allowed for the temperature to stabilize (30 min), it is extremely difficult, if not impossible, to obtain meaningful kinetic data.

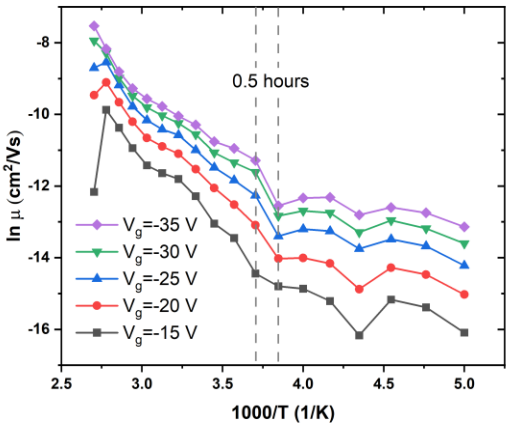

Figure 5-4 Dependence of μ on T under different V_g in medium MW RR P3HT. MW=30-50 kDa, V_d=-15 V, T=200 to 370 K. High T measurements were performed immediately after low T measurement.

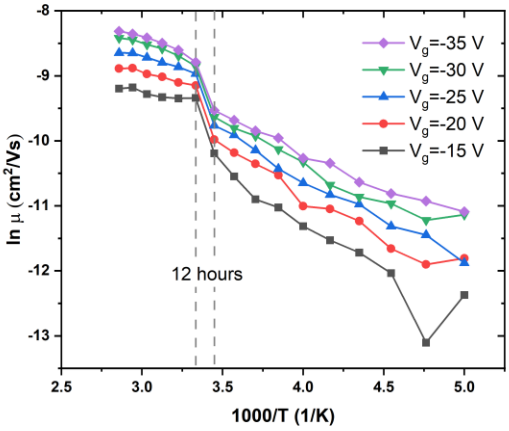

Figure 5-5 Dependence of μ on T under different V_g in medium MW RR P3HT. MW=30-50 kDa, V_d=-15V, T=200-350 K. High T measurements were performed 12 hours later than low T measurements, during which the device was left at room temperature in a vacuum probe station.

To examine our hypothesis of the glass transition, we also measured the XRD spectra of the P3HT films (a) before and (b) after the high temperature measurement, shown in Figure 5-6. We observe the same (100) diffraction peak at 2θ=5.1°, which is the typical signal of the lamellar structure of

P3HT.[58, 107] The peaks of the P3HT film after the high temperature measurement are weaker, which signifies a more amorphous thin film after the glass transition.

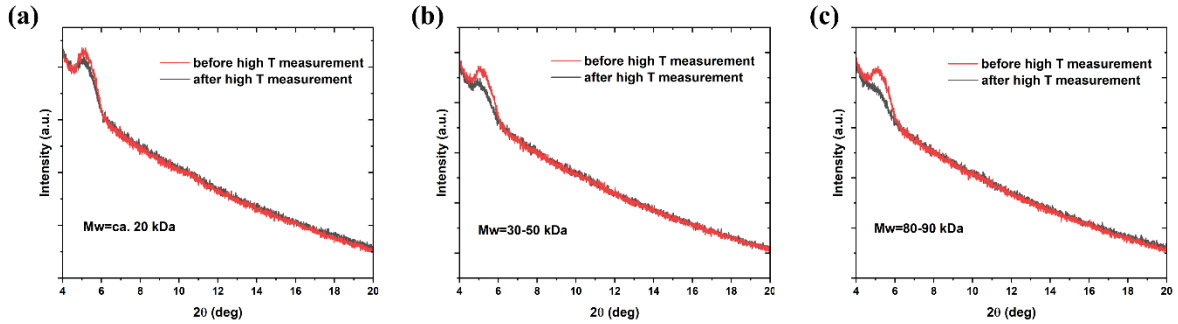

Figure 5-6 X-ray diffraction (XRD) patterns of three MW RR P3HT before and after the high T measurement.

5.5 Dependence of charge carrier density upon Vg

We determined the dependence of charge carrier density, n, on V_g at various T in high MW RR P3HT from Equation (3-9) and (3-10). As indicated in Figure 5-7, with the V_g going from 15 to 35 V, n changes by a factor of about 2 below T_α, and by twice that, above.

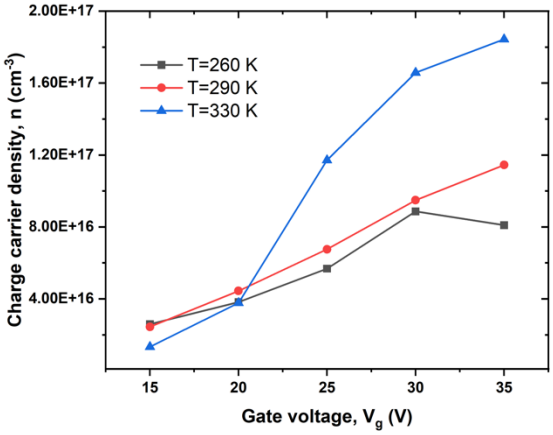

Figure 5-7 Dependence of n on V_g under different T in high MW RR P3HT, V_d=-20 V, T=260, 290 and 330 K.

5.6 Dependence of mobility upon source-drain voltage

We have determined the variation of μ with T for a given value of V_g and several values of V_d, for low, medium and high MW of P3HT. The results are presented in Figure 5-8. This behavior is independent of V_d in the range of drain-source voltages studied, at least for the low and medium MWs, that is, the behavior of the organic semiconductor and of its contacts are ohmic. This appears to render the problem of reproducibility, due to relaxation, discussed in Chapter 5.4, unimportant for this measurement, at least for low and medium MW samples. It is possible that the small scatter in Figure 5-8 (c) is due to the beginning of relaxation in the high MW material. We also note, in Figure 5-8 (b) and (c), the decrease of the apparent value of ΔE, characteristic of the α relaxation.

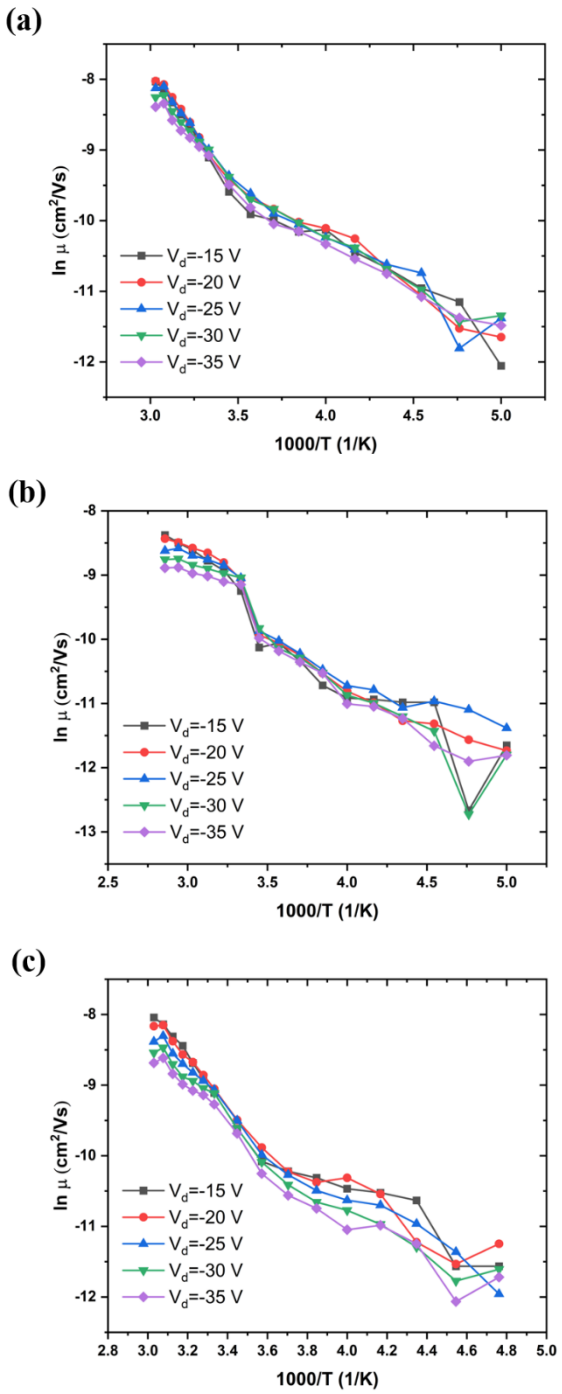

Figure 5-8 Mobility as a function of T between 200 and 350 K, (a) Low MW, ca. 20 kDa, V_g = -25 V; (b) Medium MW, 30-50 kDa, V_g = -20 V; (c) High MW, 80-90 kDa, V_g = -20 V.

For all cases, the mobility is not free-electron like (band like), it is activated. For low MW P3HT (Figure 5-8 (a), and for other values of V_g, not shown here), the activation energy for various V_g is shown in Table 5.2. For comparison, values of activation energy as a function of V_d are presented in Table 5.3. We see that the in-plane activation energy at V_g =-25 V is comparable with, but higher than those obtained in Table 5.1. We assume that the difference is due to the approximations in Equation (3-5) and (3-6), and that the mechanisms controlling mobility in both are the same: polaron hopping below T_α, and polymer backbone motion, above. As discussed in Chapter 5.4, the high temperature, WLF region, values in Table 5.1 are apparent activation energies. This is also the case in Table 5.2 and Table 5.3.

Table 5.2 Activation energy of low MW P3HT as a function of V_g, V_d=-15 V.

	V_g=-15 V	V_g=-20 V	V_g=-25 V (Fig. 6-8 (a))	V_g=-30 V	V_g=-35 V
E_a (meV) T=200-290 K	126	123	114	114	103
E_a (meV) T=290-330 K	182	243	252	290	316

Table 5.3 Activation energy of low MW RR P3HT as a function of V_d, V_g= -25 V.

	V_d=-15 V	V_d=-20 V	V_d=-25 V	V_d=-30 V	V_d=-35 V
E_a (meV) T=210-290 K	120	129	120	126	146
E_a (meV) T=290-330 K	329	282	238	219	209

5.7 AC conductivity in low MW P3HT

To shed light on inter-chain versus intra-chain hopping, we also explored transport under ac voltage on the same transistors upon which we performed dc measurements. The ac frequency provides another parameter for determining if the hopping is between chains or along chains. We expect that hopping between chains would occur only when the ac frequency is small enough and T is high enough. We measured ac conductivity, σ_{ac}, of low MW P3HT over a range of *T* from 260 K to 350 K and frequency, *f*, from 100 Hz to 1 MHz. We were unable to obtain reliable measurements below 100 Hz. At frequencies from 10 Hz to 100 Hz the values obtained changed from one measurement to the next. The standard deviation is extremely large below 100 Hz in the temperature range investigated, such that we were not able to establish a value with confidence. We take this as indicating that the relaxation frequency is comparable to the ac frequency applied and the relaxation under combined V_g and V_d is not negligible. The electric field acts on the charge carriers, which act on the polarized atoms to which they are coupled. This leads to the deformation of the molecules. The charge carriers, which can move along the molecular backbone, will hop when two molecules are close together, lowering the barrier. This process is too slow at high frequencies, and relatively efficient at dc and at low frequencies. At frequencies from 10 Hz to 100 Hz, relaxation produces uncertain positions of the carriers, resulting in a small, variable, conductivity.

Results for V_g=-20 V are shown in Figure 5-9, which also shows σ_{dc} for the same V_g, crossing the ac results. We see that σ increases with *f*, following the universal relation for disordered materials below optical frequencies.[37]

$$\sigma_{ac} = Af^s \qquad (5\text{-}1)$$

where $s \leq 1$ and can be temperature dependent.[108] However, we note that the $f = 0$, dc value may be above or below the ac values. We have also measured the dependence of σ_{ac} on V_g from -10 V to -40 V. There are small changes in σ_{ac}, of 2 to 5, which are perhaps related to the variation of charge carrier density, shown in Figure 5-7. We discuss the significance of Figure 5-9 in the following section.

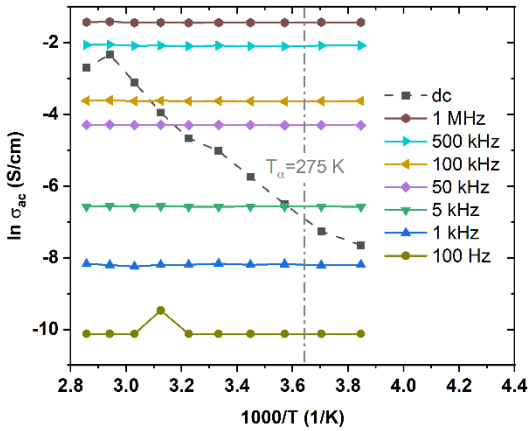

Figure 5-9 σ_{ac}, at f between 100 Hz and 1 MHz, and σ_{dc} of low MW P3HT, at T from 260 K to 350 K, V_g=-20 V.

The origin and implications of Equation (5-1) have been intensively studied. This relation is widely observed for disordered materials,[37] as noted above, and is obtained from theory for percolation on a disordered network.[43] It may be understood qualitatively from the fact that the carriers move over smaller distances about their equilibrium positions as f increases, remaining in regions of smaller variation of potential energy.

It is found experimentally in a vast majority of disordered solids that s=1 (σ_{ac} linear with f) corresponds to the Arrhenius slope, $\sigma' = \partial\sigma/\partial(1/T) = 0$.[43, 108] Theoretical models show that these two effects should occur when the process responsible for σ_{ac} makes a negligible contribution to σ_{dc}.[43, 109] As this contribution increases, s decreases and σ' increases. The data of Figure 5-9 correspond to s=1 (best fit for s=0.96), and are independent of T. In typical amorphous networks, for example, in chalcogenides,[77, 108-110] s=1 at low T, and decreases with increasing T, so that σ_{ac} increases, joining the Arrhenius line for σ_{dc}.

5.8 Discussion

In Chapter 5.4, we proposed that the mechanism controlling mobility in low T region is polaron hopping, and charge carrier hopping with polymer backbone motion in high T region.

We are now in a position to propose a mechanism for the ac conductivity, and to refine our model for the dc conductivity. In the ac measurements shown in Figure 5-9, f is low enough, and T is high enough for the charge carriers to hop on the same molecular backbone, but not enough for them to hop to other polymer chains. It indicates that the process responsible for the dc conductivity must involve relaxation frequencies, lower, in their temperature ranges of applicability, than 100 Hz, the lowest frequency investigated. As indicated above, below 100 Hz, the relaxation frequency of the glassy P3HT is comparable to *f*. The relaxation time of the low MW sample must be on the order of 0.01 sec, or higher, and is surely higher still for the higher values of MW.

That σ_{dc} can be higher than σ_{ac} also reinforces our proposal that, in the high T region, the carriers move with the polymer backbones, due to the α relaxation. They hop rapidly when two molecules approach each other. It is the backbone movements which limit the hopping rate.

In the low T regime, the carriers must also hop from molecule to molecule if they are to contribute to the dc conductivity. This happens less frequently than in the high T regime. That this process involves a relaxation implies that the hopping rate is controlled either by movement of small segments of the backbone, or by the approach of the side group on the monomer, shown in Figure 5-1, to another polymer chain. These movements involve the so-called β or γ relaxations.[56, 111] $CH_2(CH_2)_4CH_3$ is insulating.[59] Thus, carrier hopping from polymer backbone to polymer backbone must be due to the relaxation of backbone segments. That is, it is controlled by the β relaxation.

We are also able to explain the small changes in the charge carrier density with varying V_g. Contribution to σ_{dc} must require that carriers move into the band bending region. This must be difficult, but less so at high T than at low T. In contrast, the ac measurements are essentially independent of V_g. They represent the entire thickness of the semiconducting layer. This makes clear why the ac and dc results, which represent different populations in the sample, can cross over.

Our study drew a complete picture, shown in Figure 5-10, of the charge carrier transport processes in the widely studied P3HT conjugated polymer in the glassy state. The impact of polymer properties, especially relaxation, upon electronic properties has rarely been explained for organic semiconductors. We believe that the approach taken here would be useful for clarifying charge transport mechanisms in other polymeric and molecular semiconductors, well beyond P3HT. The higher mobility of the RR P3HT above the α transition temperature might also help to guide future

design of organic electronic devices. However, as indicated in the measurement of medium MW P3HT, relaxation may represent a danger to reliable device performance.

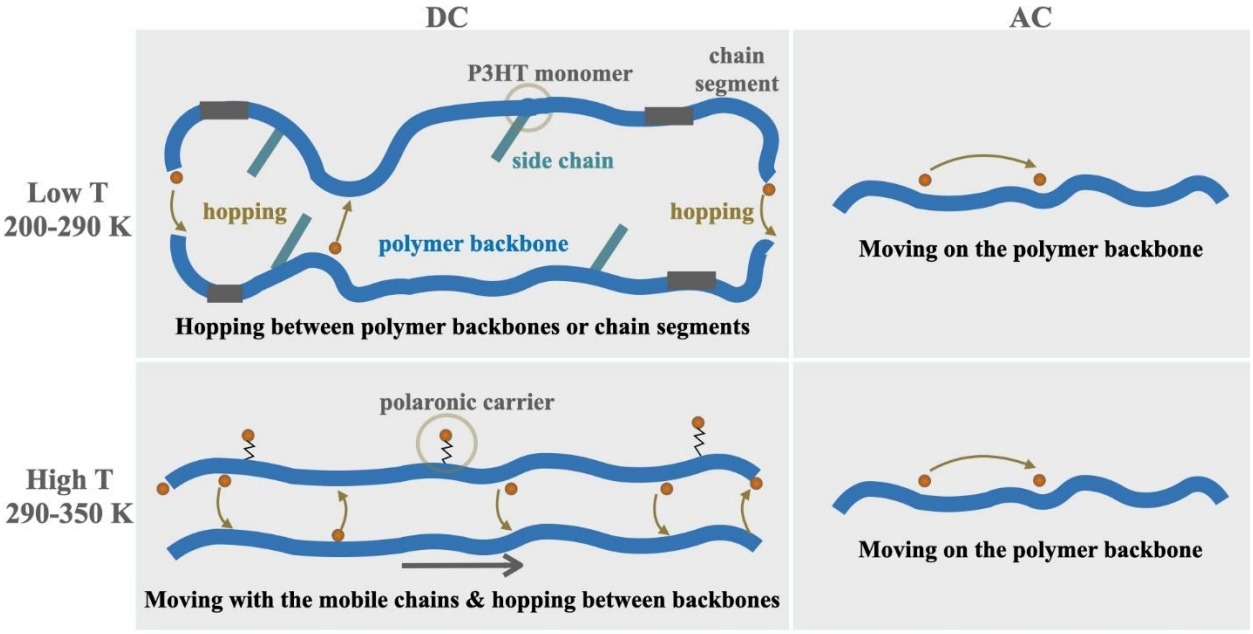

Figure 5-10 Charge carrier transport mechanisms in RR P3HT. In the low T region, the hopping is controlled by the β relaxation. In the high T region, α relaxation helps the hopping process.

It is important to recognize that, in the literature, samples of P3HT have been prepared at varying degrees of order.[31] These may not necessarily exhibit the same electronic properties. Noriega et al. have reported the results of a detailed study of semicrystalline P3HT thin film (40% ordered aggregates of the thin film, from their supplementary material) that the ordered region is more conductive than the disordered region, and that carriers need to overcome a large energy barrier to move from the ordered to amorphous region.[31] In the samples reported here, the ordered material constitutes a very small fraction (Figure 5-6). Thus, it is not sufficient for the charge carrier transport through the entire thin film. In the present case, the ordered material may make a significant contribution to the ac conduction. However, dc conduction requires percolation through the more resistive disordered region, which dominates the dc measurements.

There has been considerable work on the effect of relaxations on carrier behavior in semi-crystalline P3HT. In particular, it has been reported that relaxations scatter carriers on the molecular backbone, reducing mobility and ac conductivity.[57] Our study yields a very different insight. It demonstrates that relaxations are needed for carrier transport in glassy P3HT, the motion of carriers with the mobile polymer backbone and carriers hopping between neighboring chain segments are necessary for dc conductivity. It is likely that similar processes occur in other glassy conducting polymers. The fact that intermolecular carrier hopping requires molecular vibrations was experimentally observed in a few earlier publications,[58, 59] but not considered in detail. It may explain the observation[112] that increasing film crystallinity leads to lower mobility. This suggests that, under some circumstances, increased crystallinity could impede the approach of polymer chains and thus decrease charge carrier mobility.

Since charge carrier transport in the glassy material is closely related to polymer relaxation, detailed study of relaxation of different MW P3HT, investigation of morphology and crystallinity of the thin film after relaxation may improve our understanding on this polymer structures and the electronic properties. It would also be of interest to investigate the relaxation times or frequencies involved in the two dc conduction regimes. Given their likely values and the limitations to stability of the samples at elevated temperature, this is likely to be less difficult in the time domain than in the frequency domain. Thermally stimulated techniques might be appropriate.[113] Such studies would also permit comparison of experiment with models of the hopping process, as *s* approaches zero, and the activation energy of ac conductivity approaches that of dc conductivity. This was particularly fruitful when predictions of the correlated barrier hopping (CBH) model were compared with experiments on amorphous chalcogenides.[77, 108-110] The polaronic conduction in chalcogenide glasses was successfully described through including the MNR in the activated form in the relaxation time.

5.9 Conclusion

A positive effect of polymer molecular relaxation upon charge carrier transport processes in organic semiconductors is reported for the first time. Through studying the charge carrier transport properties of RR P3HT under various temperatures and electric fields, we reveal the correlation between polymer molecular relaxations and transport mechanisms. We find that, in the

range 200 to 290 K (low *T*), the charge carriers hop between molecules when chain segment movements (the β relaxation) permit. Between 290 K and 350 K (high *T*), charge carrier mobility increases more rapidly than it did at low *T* and is independent of V_g. We attribute this behavior to the α relaxation of the polymers, that is, to the movement of the carriers with the mobile backbones, hopping more easily than at low *T*. To shed light on inter-chain versus intra-chain hopping, we explored transport in ac conditions. The study of low MW P3HT shows that ac conductivity is independent of *T* and increases exponentially with the frequency. This indicates that carriers move freely on molecular chains in ac conditions, but that this does not contribute to dc conductivity.

The transport mechanisms in glassy P3HT is explained unambiguously for the first time. This should contribute to advances in P3HT materials synthesis as well as technological developments for thermally stable organic photovoltaics, organic thermoelectrics, and thermally triggered degradable electronics. We believe that the dependence of charge carrier transport on molecular relaxations is unlikely to be limited to P3HT. The approach taken here is expected to pave the way to discover analogous molecular relaxation properties in other organic polymeric semiconductors.

CHAPTER 6 CHARGE CARRIER TRANSPORT IN A SEMICONDUCTOR BASED ON A SMALL ORGANIC MOLECULE: PHENYL-C61-BUTYRIC ACID METHYL ESTER (PCBM)

6.1 Introduction

Although PCBM is a prototype n-type small molecule widely used as electron acceptor in OPV, the pristine material has been poorly studied. Solution-processed thin films of PCBM are usually structurally and energetically disordered due to the high concentrations of defects (owing to the inherent properties of organic materials, inclusion of impurities and solvent molecules).[30] This leads to difficulty in understanding the charge carrier transport process.[45, 114, 115]

MNR in PCBM has previously been studied by Fishchuk et. al [116] and by von Hauf [117]. Fishchuk et. al. [116] studied the dependence of charge carrier mobility on T without changing the gate voltage. von Huaf[117] investigated the charge injection conditions with various metal contacts. Mg contacts exhibited the best charge injection due to the doping of Mg into the fullerene derivatives and to MgO bilayer formation at the interface of the metal contact and the semiconductor. The field effect carrier mobility of PCBM was studied by modulating ΔE by varying the gate voltage. However, measurements were reported for only two gate voltages, with extrapolation over different temperatures. Here, we report a more thoroughly study, whose motivation is to use the Arrhenius plot to cast light on the conduction mechanisms of PCBM, as we have done for P3HT in Chapter 5.

Schottky barrier formation between the metal electrode and the LUMO or HOMO level of the semiconductor (depending upon the sign of the carriers in the semiconductor) limits the injection efficiency of the transistors. Structural disorder and interfacial traps also affect injection efficiency. A strong electrostatic field at the electrode-semiconductor interface improves injection efficiency. 1D SWCNT with one end connected to a metal contact and the other to PCBM provides such an electrostatic effect. SWCNT arrays improve the charge injection and charge carrier mobility as compared to conventional Au electrodes. The linear mobilities of SWCNT based OTFTs and Au based OTFTs were 2×10^{-2} cm^2/Vs and 1×10^{-3} cm^2/Vs.[28]

This chapter is devoted to the study of the dependence of charge carrier transport process upon the temperature and upon details of the crystal structure of the PCBM film. To gain insight into the fundamental properties, we optimized the performance of PCBM based OFETs by reducing electron trapping at the dielectric-semiconductor interface and by increasing charge carrier injection through embedding SWCNTs into the conventional gold electrode. We then used MNR to investigate charge carrier transport mechanisms in PCBM thin films.

6.2 Optimization of PCBM thin film performance: influence of HMDS, thermal treatment, air exposure and SWCNT on charge carrier injection

Chua et al. demonstrated that electron trapping by hydroxyl groups at the untreated dielectric-PCBM interface leads to poor OFET characteristics.[118] As shown in Figure 6-1, the drain-source current is extremely low due to the electron trapping at dielectric-PCBM interface, and the transistor character is not obvious. To overcome this problem, Chua et al. replaced the commonly used dielectric material SiO_2 with high quality hydroxyl-free dielectric material, such as divinyl tetramethyl siloxane-bis(benzocyclobutene) derivative (BCB) and found that the performance of n-type material-based devices improved significantly. Another method is hexamethyldisilazane (HMDS) coating, HMDS can break the O-H bond and form O-Si$(CH_3)_3$, which greatly limits trapping at the interface. According to our study, the current in the PCBM-based devices after HMDS treatment increases 2 orders of magnitude and a clear n-type transistor behavior appears.

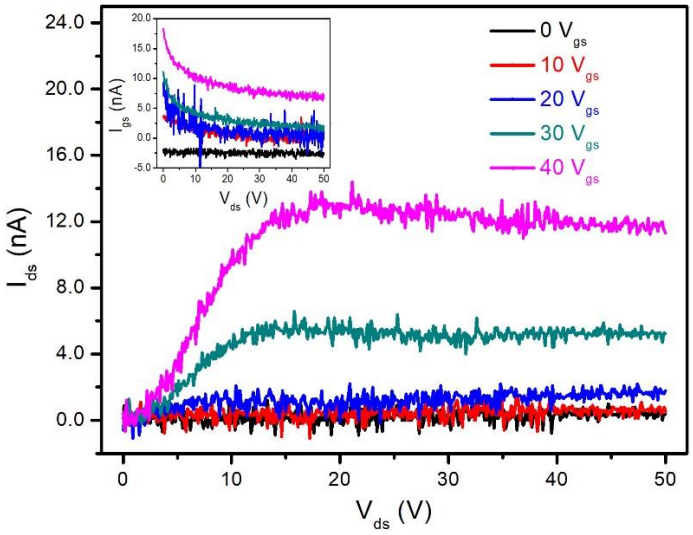

Figure 6-1 Output curves of a PCBM-based FET, measured at room temperature.

We find that HMDS, thermal treatment and exposure to ambient air will all influence device performance. Therefore, we have studied six groups of samples in different conditions with HMDS, thermal treatment, and exposure to ambient air (overnight) as parameters. Transfer curves of PCBM-based devices: (1) without HMDS and thermal treatment, stored in the N_2 glovebox; (2) after thermal treatment but without HMDS, stored in the N_2 glovebox; (3) after HMDS but without thermal treatment, stored in the N_2 glovebox; (4) with both HMDS and thermal treatment, stored in the N_2 glovebox; (5) after HMDS but without thermal treatment, exposed to ambient air and (6) without HMDS and thermal treatment, exposed to ambient air were studied. The results showed that groups (2) thermal treatment, no HMDS, no ambient air exposure; sample (3) with HMDS, no thermal treatment, no ambient air exposure and sample (4) with HMDS and thermal treatment, no ambient air exposure have the best performance.

Here we show results of groups (2), (3) and (4) mentioned above, using HMDS and thermal treatment as varying parameters. Four sets of samples are shown in Figure 6-2.

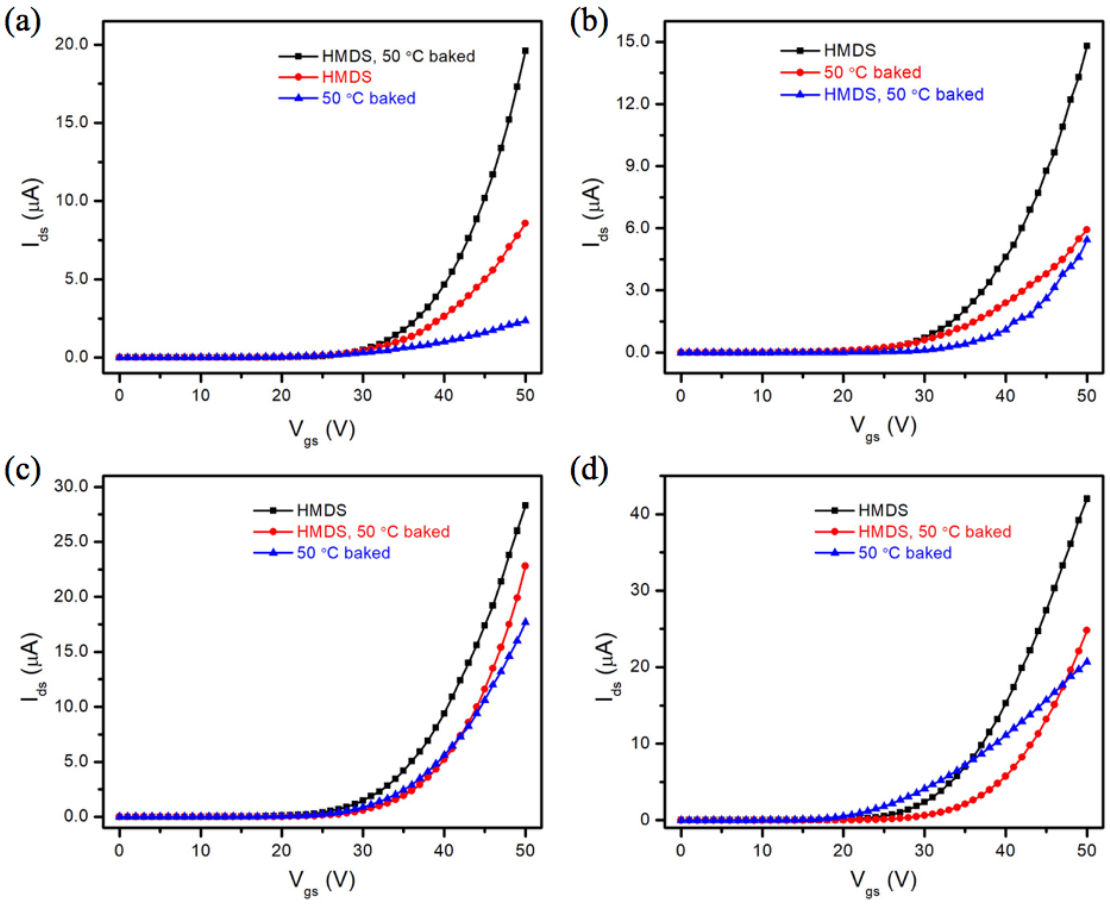

Figure 6-2 Transfer curves of PCBM devices with HMDS coating and thermal treatment as parameters, all curves are scanned at V_d=50 V.

In general, samples with HMDS have better performance. But whether thermal treatment is good for samples or not can still not be decided. We studied both of them and calculated the charge carrier mobility. The average mobility of devices with both HMDS and thermal treatment is μ=0.0019 $\pm$ 0.0011 cm^2/Vs. While the mobility of devices after HMDS treatment but without thermal treatment is μ=0.0016 $\pm$ 0.0008 cm^2/Vs.

We fabricated the electrodes with SWCNTs to further improve charge carrier injection. The SWCNT electrodes consist of bundles of SWCNTs having one end in the channel and the other, connected to the electrode. SEM images of SWCNT electrodes are shown in Figure 6-3.

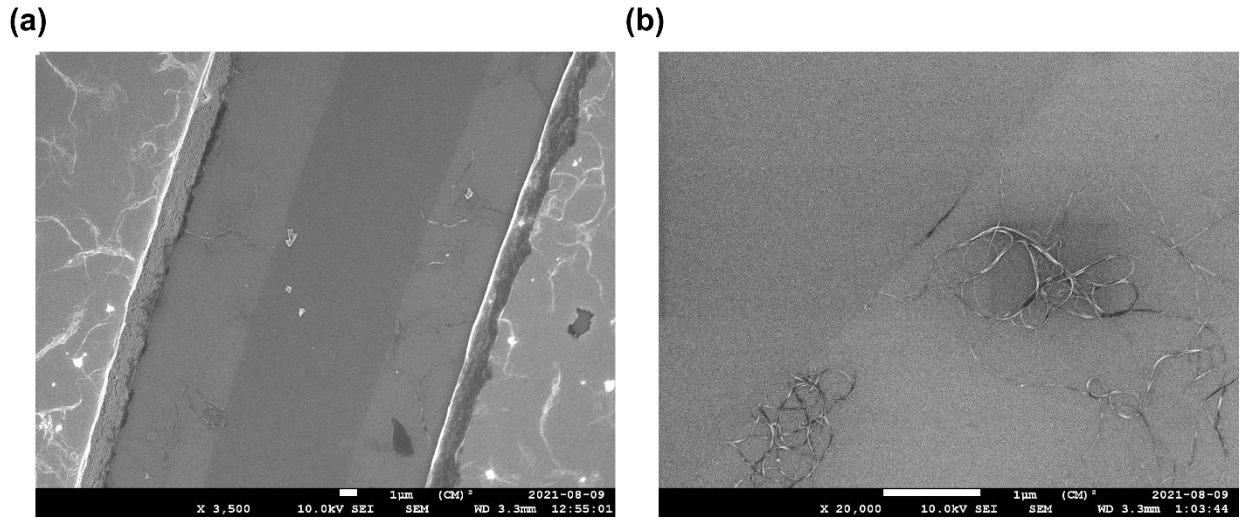

Figure 6-3 The SEM images of the (a) Au electrode coated on SWCNTs/SiO_2 substrate and (b) SWCNT tails with etching profile in the channel.

Figure 6-4 shows the output curve of PCBM thin film fabricated on the conventional device and SWCNTs-based device. Compared to the device fabricated with gold electrode (Figure 6-4 (a)), the current of the SWCNTs-based device is improved approximately 3 orders of magnitude (Figure 6-4 (b)). It demonstrates that the SWCNT arrays provide better electron injection.

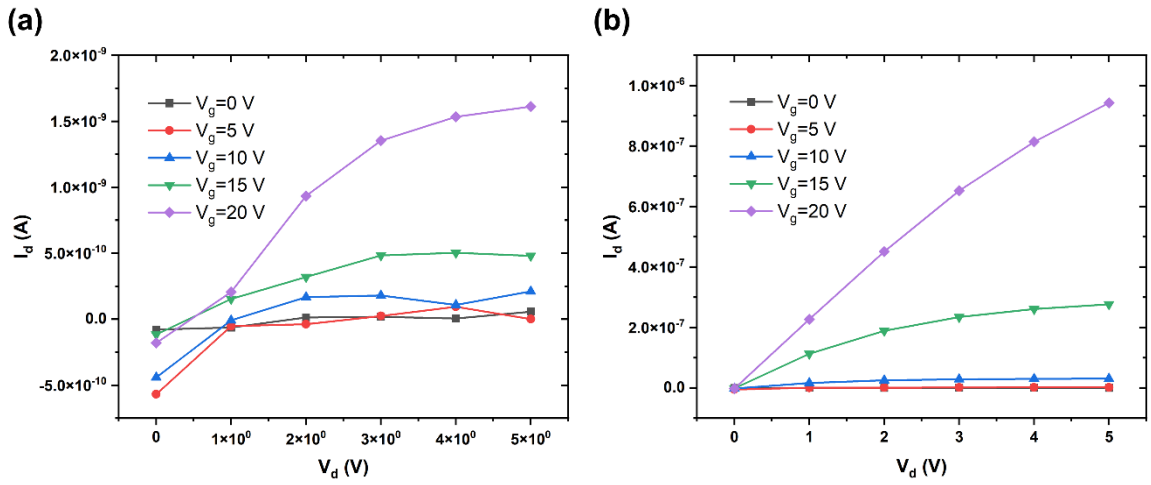

Figure 6-4 The output curve of the PCBM-based device with (a) conventional gold electrode (b) SWCNTs-based electrode.

6.3 Dependence of mobility on T under several V_g in conventional Au based OFET and SWCNT/Au-based FET

By modifying the semiconductor-dielectric interface and improving the charge carrier injection, we optimized the devices for study of the charge carrier transport mechanisms in PCBM. The dependence of μ upon *T* for several V_g is then studied in Figure 6-5.

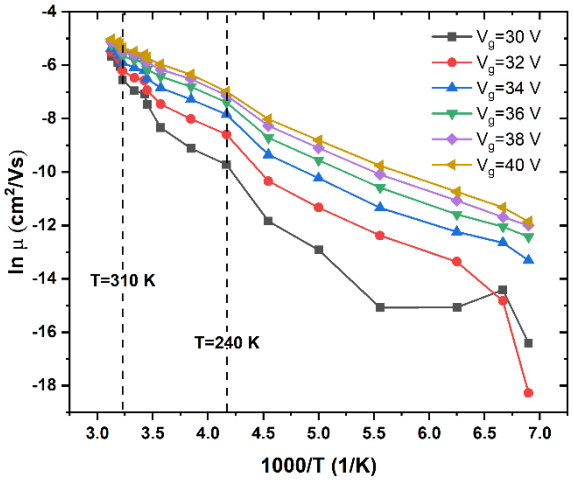

Figure 6-5 Arrhenius plot for PCBM based OFET, with V_d=10 V. T varies from 145 to 320 K.

As shown in Figure 6-5, at T<240 K, μ increases with V_g and depends exponentially upon T at a given V_g. The activation energies, shown in Table 6.1, are calculated from the data in Figure 6-5, using Equation (2-1).

Table 6.1 Activation energy in PCBM-based FET as a function of V_g.

	Ea (meV) T=145-240 K	**Ea (meV) T=260-310 K**	**Ea (meV) T=312-320 K**
Vg=30 V	168	377	383
Vg=32 V	243	264	303
Vg=34 V	156	201	254
Vg=36 V	149	167	202
Vg=38 V	147	150	166

Vg=40 V	145	142	175

As we may see, the activation energies for PCBM thin films are considerably higher than excitation and thermal energies. This would be in agreement with the multi-excitation entropy model and support it as the explanation of the origin of MNR.[65, 92] At $T > 240$ K, μ increases more rapidly as a function of 1/T than at lower temperature. This increase becomes more rapid at T=310 K, with μ becoming less dependent upon V_g. This rapid increase of the μ signifies the decrease of the activation barrier. We attribute this change in Arrhenius slope to the crystallization of the PCBM small molecules under elevated temperature.[119, 120] In the low temperature (145-240 K) region, the charge carrier hops between PCBM molecules in a mostly amorphous thin film. As we shall show, in the high temperature (240-320 K) region, PCBM molecules can diffuse, increasing the crystallinity.[120] The increased crystallinity of the film facilitates electron hopping. This is illustrated in Figure 6-6.

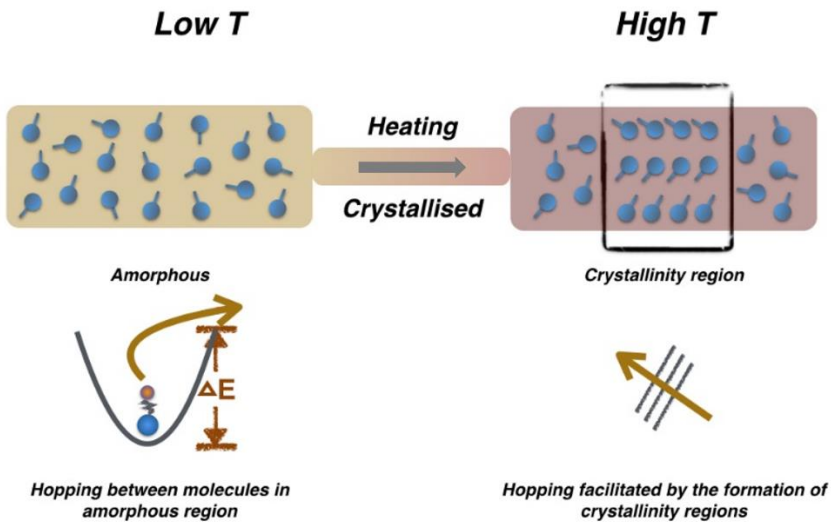

Figure 6-6 Hypothesis of effect of T on film structure and charge carrier transport in PCBM thin film.

6.4 Structural changes in PCBM

To pursue this hypothesis that the PCBM crystallized as described in the previous chapter, we performed grazing X-ray diffraction (XRD) measurements before and after high temperature measurement. The results of the XRD measurements are shown in Figure 6-7. The three diffraction peaks in the figure are at 2θ=3.8°(corresponding to an interplanar distance of 2.3 nm), 5.2° (1.7 nm), 6.5° (1.4 nm).[121] According to the Scherrer relation,[122] the mean size of the crystallites of these three peaks are 25.4, 2.8, and 1.4 nm, respectively. Comparing with the sample before high T measurement, the peak at 3.8° is sharper, which gives ca. 1.6 nm larger crystallized region in the thin film. The new peak located at 5.2° also demonstrates our proposal that the crystallization process happens with the T increases.

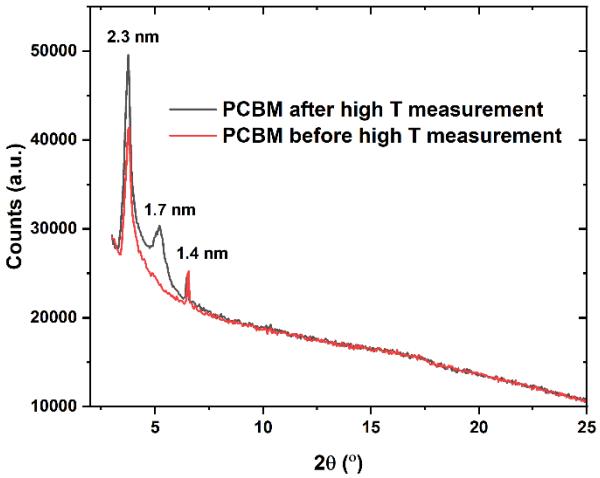

Figure 6-7 XRD patterns of PCBM films on SWCNT/Au electrode fabricated on HMDS treated substrate.

6.5 Electrical measurement of PCBM-based FET during three heating and cooling cycles

We also measured μ as *T* increased during three heating and cooling cycles. The 2nd cycle was carried out immediately after the 1st cycle, and the 3rd cycle, 12 h after the 2nd cycle. As shown in

Figure 6-8, μ increased in both cycles. This increase in the 2nd cycle is attributed to the crystallization process. The further improved in the 3rd cycle is probably due to the relaxation of the PCBM molecules. The drop of the curve at high T under V_g=20 and 30 V is due to the scattering of charge carriers. Some electrons are deviated from their original path for hopping under high temperatures. While at higher V_g, more electrons are induced, the effect of the electric field suppresses the effect of scattering.

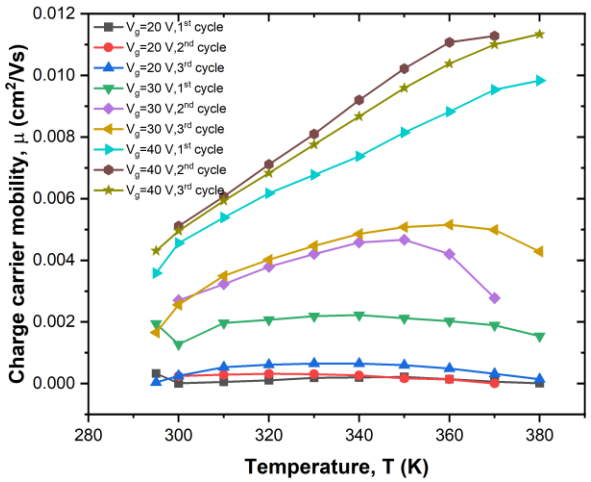

Figure 6-8 Effect of cycling measurements in PCBM-based FET, V_d=10 V, T=295 to 380 K, samples were kept in a vacuum probe station.

6.6 Discussion

The study of high-performance n-type organic semiconductors is essential to complementary logic circuits fabrication. However, there are three obstacles before organic n-type organic transistors. First, the noble metals, e.g. Au, Ag, mainly used in electrodes have work functions which are more suitable for injection of holes into the HOMO level, rather than into the LUMO level, for typical organic semiconductors. Although lower work function metals like Mg and Ca have lower Schottky barriers, which can ensure better electron injection from the electrodes, they are more reactive with the organic semiconductors and are easily oxidized. Second, oligoacenes and oligothiophenes have relatively small electron affinities, and, although the molecules can be chemically tuned with electron withdrawing side groups to transport electrons more efficiently, the final compounds are

more sensitive to the atmosphere.[94] Third, electrons are trapped at the semiconductor-dielectric interface by hydroxyl groups, present in the silanol groups in the most frequently used dielectric, SiO_2. These three effects have rendered n-type transistors elusive. Here, following the literature, we have coated HMDS on the SiO_2 gate dielectric to decrease the electron trapping at the dielectric interface with the PCBM film. SWCNTs were successfully embedded in the conventional gold electrodes to form a strong electrostatic field at the electrode-semiconductor interface to improve the electron injection efficiency.

The dependence of charge carrier transport behavior upon crystal structure and its stability under various temperatures was then studied, PCBM crystallization processes are found during the measurement.

It has been shown that the annealed PCBM films can be converted to ambipolar material after vacuum annealing at 400 K for several hours.[28] It would be of interest to study the charge carrier transport properties of electrons and holes in PCBM thin films and compare charge transport mechanisms before and after the conversion of polarity of the thin film.

The detailed study of the structure and the packing of the PCBM small molecules under different temperatures would also help us to identify that if there is a favorable stacking for electron transport. Such understanding would contribute to the material synthesis of thermally stable OPV and OTFTs.

6.7 Conclusion

The fullerene-based derivative phenyl-C61-butyric acid methyl ester (PCBM) has attracted attention as a transistor channel and organic photovoltaic material, due to its solution processability, stability and high electron mobility. However, disorder in solution processed PCBM thin films makes understanding of charge carrier transport mechanisms difficult. We have fabricated PCBM based FETs and improved device performance by reducing the electron trapping at the dielectric-semiconductor interface and improving charge carrier injection. SWCNTs were successfully integrated into conventional gold electrodes to improve injection efficiency. The charge carrier mobility was improved by about three orders of magnitude. Arrhenius plot has been employed to cast light on charge carrier transport mechanisms in PCBM film. Crystallization of

PCBM was observed during the measurement. At low temperature, charge carriers hop between molecules in the amorphous region. At high temperature, this hopping is facilitated by the formation of more crystallized regions.

CHAPTER 7 GENERAL DISCUSSION

In the past two decades, research in organic semiconductors has been focused on increasing the crystallinity degree in order to achieve higher device performances.[123-126] Thus, semi-crystalline films[31-35, 127] have been thoroughly studied, while amorphous organic materials have been neglected. Here, we present an investigation of charge carrier transport in amorphous P3HT and PCBM films. These have been incorporated into transistors, permitting control of a wide range of parameters: temperature, gate voltage, drain source voltage, and AC frequency. Typical investigations have involved a limited range of these parameters. We have used the widest range possible. This has permitted us to explain the charge carrier transport mechanism in P3HT film unambiguously and figure out the change of the charge carrier transport mechanism in low and high temperature region in PCBM film.

Charge carrier transport in glassy P3HT was studied under DC and AC conditions. DC charge carrier transport mechanism is determined by the Arrhenius plot. The MNR behavior in the DC conditions shows that polaronic conductors hop in the low temperature region. In the high temperature region, the charge carriers obey WLF instead of MNR, indicating the effect of molecular relaxation: charge carriers hop with the polymer backbone motions, bringing about a decrease of the activation barrier. DC measurements cannot provide more insight about how charge carriers hop in the low temperature region. AC measurements have therefore been performed on the same sample to provide another parameter, the frequency, to shed light on the inter- or intra-chain hopping. It has been found that the frequency is low enough and the temperature is high enough for charge carriers to hop on the same polymer backbone; charge carriers cannot hop to other polymer chains in AC conditions. The fitting of AC results with the universal relation regarding the dependence of conductivity on frequency found in disordered materials show that the AC conductivity makes a negligible contribution to the DC conductivity. These results help us to refine the charge carriers hopping mechanism in DC condition: the charge carriers must hop between polymer chains when chain segments approach each other.

The effect of relaxation on intermolecular charge transfer is much greater than the scattering effect. This thesis fills in a blank: the charge transfer from molecule to molecule in the glassy polymer, necessary for DC conductivity, requires molecular relaxations. Actually, the positive effect of relaxation on charge carrier mobilities has been experimentally reported in a few publications but

not considered in detail.[7-8] Efforts were focused on device performance or the effect of scattering at high temperatures. The higher mobility of the RR P3HT above the α transition temperature might help to guide future design of organic electronic devices. For instance, systematically increasing crystallinity of the organic semiconductors may finally impede the approach of polymer chains and thus decrease charge carrier mobility at high temperatures. Most importantly, this result proposed an approach which might be useful for clarifying charge carrier transport mechanism in other glassy polymers. Possible continuations of this work are

1. Time-domain measurements of low frequency conductivity of P3HT

Since charge carrier transport in the glassy material is closely related to polymer relaxation, it would be of interest to investigate the relaxation times or frequencies involved in the low temperature and high temperature regions in P3HT. It is likely to be accomplished through changing the waiting time during the measurement instead of changing the ac frequency. The acquisition of the detailed values of the relaxation time at different temperatures may permit the comparison of the experiments with theoretical models of hopping process. F. Abdel-Wahab et. al.[110] studied the dependence of dc and ac conductivity on temperature and frequency in chalcogenide glasses, and found that the experimental data fits very well with the modified bi-polaron correlated barrier hopping (CBH) model, which includes the MNR term in the relaxation time.[77, 108-110] The polaronic conduction in chalcogenide glasses was successfully described through this theoretical model. It solved the debate that the transport mechanism in this material is band transport, electron tunneling through intermolecular barrier, polaron hopping or other models.[85]

2. The study of thiophene with a conjugated side chain

The study of a polymer which is similar to P3HT but with a conjugated side chain instead of the insulating alkyl chain would also be of interest. The monomer of 3-Phenylthiophene, shown in Figure 7-1, might be a good candidate. It is expected that it would have a higher DC conductivity than P3HT at low temperatures. It might show a similar AC conductivity behavior to that of P3HT at high frequencies, but may start to deviate from P3HT result at low frequencies. If it is demonstrated, it might guide the design of side chains in organic semiconductors: In glassy

polymers, the side chain can not only be used as solubilizing groups or groups which tune the physical properties, it can also enhance the charge transport through molecular relaxation.

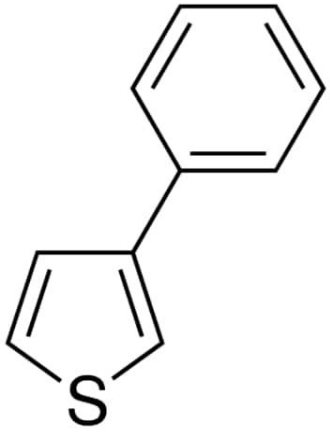

Figure 7-1 Monomer of 3-Phenylthiophene.

3. Validation of positive effect of molecular relaxations on other glassy polymers

It is unlikely that this positive effect of relaxation on charge carrier transport is limited to P3HT. In the future, we should explore more glassy polymers to see if this conclusion can be generalized to other disordered materials. DC measurement might help to explain the charge carrier transport process both above and below the glass transition temperature. AC measurement might provide insights of detailed transport mechanisms, e.g. polaron hopping (along or between the chains), electron tunneling or percolation. The difficulty of this project is in choosing the materials and how to avoid the scattering effect. The candidate polymer should have high charge carrier mobility and good thermal stability so that the meaningful kinetics can be measured at a wide range of temperatures. N-annulated perylene tetraester (PTEN-H), shown in Figure 7-2, might be a good choice, it shows a good thermal stability at least up to 330 °C.[128] α relaxations are especially sensitive to the thermal pretreatments,[129-131] the high temperature stability of the material would allow a wide range of thermal annealing temperature, thus modifying the alpha relaxation temperature. The amorphous PTEN-H thin films can be obtained by spin coating techniques.[132] It will permit the study of molecular relaxation effect on charge carrier transport in this glassy material. Bromination of PTEN-H allows the structural modification of the monomer,[133] the

electron-donating pyrrolidine or electron withdrawing cyano can then be added to the PTEN-H molecules. The charge carrier transport mechanism can then be tuned through the side chain modifications.

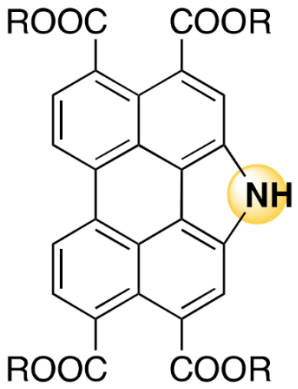

Figure 7-2 Molecular structure of PTEN-H.

In the study of the charge carrier transport in small molecule semiconductor PCBM, we observed a change of charge carrier transport mechanisms between low and high temperature regions, the motion of small molecules influenced the transport. We found the charge carrier mobility of PCBM thin film increased in both the 2nd and 3rd cycle in the heating and cooling cycling tests in Chapter 6. The increase of the mobility in the 2nd cycle is attributed to the crystallization of the PCBM thin film. In the 3rd cycle, this increase is probably due to the molecular relaxations. Further studies which need to be performed are

1. The measurement of AC conductivity in PCBM thin film

It may improve our understanding of the effect of molecular relaxations on charge carrier transport. The study of AC conductivity under different temperatures and frequencies might also indicate the detailed charge carrier transport mechanisms in PCBM.[110]

2. The study of ambipolar property of PCBM

It was shown by some researchers that PCBM thin films can be converted to ambipolar by vacuum annealing the samples at 400 K for several hours.[28] The charge carrier transport properties of electrons and holes in the PCBM and the comparison of charge transport mechanisms before and

after the conversion of polarity of the thin film might be of interest. This high temperature annealing procedure might also increase the tolerance of PCBM thin film at high temperatures. The aim of measuring the mobility of PCBM at higher temperatures without being affected by strong electron scattering might be achieved. It could help us to gain insight into a complete picture of charge carrier transport mechanisms in this small molecular organic semiconductor.

CHAPTER 8 CONCLUSION

The conduction mechanisms in organic semiconductor P3HT and PCBM are clarified by exploiting Meyer-Neldel rule. The activation energy of the charge carriers is modified by varying gate voltage in FET. We find that intermolecular charge transfer in glassy material is needed for the current to traverse the transistor channel. The importance of molecular motions to electronic transport in amorphous organic semiconductors is shown clearly for the first time.

It is observed that carrier mobility in P3HT depends upon Vg below the glass transition temperature but is independent of it above. It is due to the α relaxation of the polymer. At temperatures above T_α, the hole-like polaronic carriers hop between, and move with the mobile polymer backbones. Below T_α, the carriers hop between chain segments of essentially immobile neighboring molecules. Under drain voltage at frequencies higher than 100 Hz, charge carriers move freely on polymer chains. This motion along the polymer chain does not contribute to dc conductivity.

We fabricated PCBM based organic field effect transistors and improved device performance by reducing the electron trapping at the dielectric-semiconductor interface and improving charge carrier injection. Carbon nanotubes were successfully integrated into the conventional gold electrode to improve the injection efficiency. The charge carrier mobility of devices was improved by about three orders of magnitude compared to the device with untreated SiO_2 substrate and gold electrode. The study of Meyer-Neldel behavior shows that the charge carrier transport behavior changed at high temperature region, and X-ray Diffraction results indicates that crystallization of PCBM small molecule occurred during the measurement. At low temperature, the charge carriers hop between molecules in the amorphous region. At high temperature, the amorphous material is annealed, resulting in the formation of more crystallized regions. The crystallization is irreversible, so that low temperature conduction is also improved.

The transport mechanisms in amorphous P3HT is explained unambiguously for the first time. This clear picture of charge carrier transport mechanisms under different conditions will guide the design of stacking and orientation of organic semiconductors in material synthesis. We believe that the dependence of charge carrier transport on molecular relaxations is unlikely to be limited to these two materials. The approach taken here is expected to pave the way to discover analogous molecular relaxation properties in other organic semiconductors. Insights into the dependence of

charge carrier transport properties upon the molecular properties should contribute to advances in stable OPV, OLED, OTFT, organic thermoelectrics, and thermally triggered vanishing electronics.

REFERENCES

1. Shirakawa, H.; Louis, E. J.; MacDiarmid, A. G.; Chiang, C. K.; Heeger, A. J., Synthesis of electrically conducting organic polymers: halogen derivatives of polyacetylene,(CH) x. *Journal of the Chemical Society, Chemical Communications* **1977,** (16), 578-580.
2. Cicoira, F.; Santato, C., *Organic electronics: emerging concepts and technologies*. John Wiley & Sons: Weinheim, Germany, 2013.
3. Forrest, S. R., *Organic electronics: foundations to applications*. Oxford University Press: Oxford, United Kingdom, 2020.
4. Klauk, H., *Organic electronics II: more materials and applications*. John Wiley & Sons: Weinheim, Germany, 2012.
5. Ogawa, S., *Organic Electronics Materials and Devices*. Springer: Tokyo, Japan, 2015.
6. Lee, K. S.; Smith, T. J.; Dickey, K. C.; Yoo, J. E.; Stevenson, K. J.; Loo, Y. L., High - Resolution Characterization of Pentacene/Polyaniline Interfaces in Thin - Film Transistors. *Advanced Functional Materials* **2006,** *16* (18), 2409-2414.
7. Paterson, A. F.; Singh, S.; Fallon, K. J.; Hodsden, T.; Han, Y.; Schroeder, B. C.; Bronstein, H.; Heeney, M.; McCulloch, I.; Anthopoulos, T. D., Recent progress in high - mobility organic transistors: a reality check. *Advanced Materials* **2018,** *30* (36), 1801079.
8. Templier, F., From Amorphous-Si Thin-Film-Transistors to Single Crystal-Si Transistors: Influence of Si Crystallinity on Device Properties. *ECS Transactions* **2009,** *22* (1), 49.
9. Khouri, T.; Zeitler, U.; Reichl, C.; Wegscheider, W.; Hussey, N.; Wiedmann, S.; Maan, J., Linear magnetoresistance in a quasifree two-dimensional electron gas in an ultrahigh mobility GaAs quantum well. *Physical Review Letters* **2016,** *117* (25), 256601.
10. Cosseddu, P.; Caironi, M., *Organic Flexible Electronics: Fundamentals, Devices, and Applications*. woodhead publishing: Cambridge, United Kingdom, 2021.
11. Kim, S. H.; Hong, K.; Xie, W.; Lee, K. H.; Zhang, S.; Lodge, T. P.; Frisbie, C. D., Electrolyte - gated transistors for organic and printed electronics. *Advanced Materials* **2013,** *25* (13), 1822-1846.
12. Yang, H.; Shin, T. J.; Yang, L.; Cho, K.; Ryu, C. Y.; Bao, Z., Effect of mesoscale crystalline structure on the field - effect mobility of regioregular poly (3 - hexyl thiophene) in thin - film transistors. *Advanced Functional Materials* **2005,** *15* (4), 671-676.
13. Ji, D.; Li, T.; Liu, J.; Amirjalayer, S.; Zhong, M.; Zhang, Z.-Y.; Huang, X.; Wei, Z.; Dong, H.; Hu, W., Band-like transport in small-molecule thin films toward high mobility and ultrahigh detectivity phototransistor arrays. *Nature communications* **2019,** *10* (1), 1-8.
14. Horowitz, G.; Delannoy, P., An analytical model for organic - based thin - film transistors. *Journal of Applied Physics* **1991,** *70* (1), 469-475.
15. Lu, N.; Li, L.; Banerjee, W.; Sun, P.; Gao, N.; Liu, M., Charge carrier hopping transport based on Marcus theory and variable-range hopping theory in organic semiconductors. *Journal of Applied Physics* **2015,** *118* (4), 045701.
16. Lu, N.; Li, L.; Liu, M., Universal carrier thermoelectric-transport model based on percolation theory in organic semiconductors. *Physical Review B* **2015,** *91* (19), 195205.
17. Yamamoto, T.; Komarudin, D.; Arai, M.; Lee, B.-L.; Suganuma, H.; Asakawa, N.; Inoue, Y.; Kubota, K.; Sasaki, S.; Fukuda, T., Extensive studies on π-stacking of poly (3-alkylthiophene-2, 5-diyl) s and poly (4-alkylthiazole-2, 5-diyl) s by optical spectroscopy, NMR

analysis, light scattering analysis, and X-ray crystallography. *Journal of the American Chemical Society* **1998,** *120* (9), 2047-2058.
18. Neto, N. M. B.; Silva, M. D.; Araujo, P. T.; Sampaio, R. N., Photoinduced Self-Assembled Nanostructures and Permanent Polaron Formation in Regioregular Poly (3-hexylthiophene). *Advanced Materials* **2018,** *30* (16), 1705052.
19. Chiguvare, Z.; Parisi, J., Current conduction in poly (3-hexylthiophene) and in poly (3-hexylthiophene) doped [6, 6]-phenyl c61-butyric acid methylester composite thin film devices. *Zeitschrift für Naturforschung A* **2012,** *67* (10-11), 589-600.
20. Nawaz, A.; Kumar, A.; Hümmelgen, I. A., Ultra-high mobility in defect-free poly (3-hexylthiophene-2, 5-diyl) field-effect transistors through supra-molecular alignment. *Organic Electronics* **2017,** *51*, 94-102.
21. Hutchison, G. R.; Ratner, M. A.; Marks, T. J., Hopping transport in conductive heterocyclic oligomers: reorganization energies and substituent effects. *Journal of the American Chemical Society* **2005,** *127* (7), 2339-2350.
22. Grozema, F. C.; Van Duijnen, P. T.; Berlin, Y. A.; Ratner, M. A.; Siebbeles, L. D., Intramolecular charge transport along isolated chains of conjugated polymers: effect of torsional disorder and polymerization defects. *The Journal of Physical Chemistry B* **2002,** *106* (32), 7791-7795.
23. Nagamatsu, S.; Pandey, S. S., Ordered arrangement of F4TCNQ anions in three-dimensionally oriented P3HT thin films. *Scientific reports* **2020,** *10* (1), 1-10.
24. Larson, B. W.; Whitaker, J. B.; Popov, A. A.; Kopidakis, N.; Rumbles, G.; Boltalina, O. V.; Strauss, S. H., Thermal [6, 6]→[6, 6] isomerization and decomposition of PCBM (phenyl-C61-butyric acid methyl ester). *Chemistry of Materials* **2014,** *26* (7), 2361-2367.
25. Larson, B. W.; Whitaker, J. B.; Wang, X.-B.; Popov, A. A.; Rumbles, G.; Kopidakis, N.; Strauss, S. H.; Boltalina, O. V., Electron affinity of phenyl–C61–butyric acid methyl ester (PCBM). *The Journal of Physical Chemistry C* **2013,** *117* (29), 14958-14964.
26. Boucher, D.; Howell, J., Solubility characteristics of PCBM and C60. *The Journal of Physical Chemistry B* **2016,** *120* (44), 11556-11566.
27. Kanbara, T.; Shibata, K.; Fujiki, S.; Kubozono, Y.; Kashino, S.; Urisu, T.; Sakai, M.; Fujiwara, A.; Kumashiro, R.; Tanigaki, K., N-channel field effect transistors with fullerene thin films and their application to a logic gate circuit. *Chemical physics letters* **2003,** *379* (3-4), 223-229.
28. Cicoira, F.; Aguirre, C. M.; Martel, R., Making contacts to n-type organic transistors using carbon nanotube arrays. *ACS nano* **2011,** *5* (1), 283-290.
29. Xie, Q.; Perez-Cordero, E.; Echegoyen, L., Electrochemical detection of C606-and C706-: Enhanced stability of fullerides in solution. *Journal of the american chemical society* **1992,** *114* (10), 3978-3980.
30. Paterno, G.; Warren, A. J.; Spencer, J.; Evans, G.; Sakai, V. G.; Blumberger, J.; Cacialli, F., Micro-focused X-ray diffraction characterization of high-quality [6, 6]-phenyl-C 61-butyric acid methyl ester single crystals without solvent impurities. *Journal of Materials Chemistry C* **2013,** *1* (36), 5619-5623.
31. Noriega, R.; Rivnay, J.; Vandewal, K.; Koch, F. P.; Stingelin, N.; Smith, P.; Toney, M. F.; Salleo, A., A general relationship between disorder, aggregation and charge transport in conjugated polymers. *Nature materials* **2013,** *12* (11), 1038-1044.

32. Bao, Z.; Dodabalapur, A.; Lovinger, A. J., Soluble and processable regioregular poly (3-hexylthiophene) for thin film field-effect transistor applications with high mobility. *Applied physics letters* **1996,** *69* (26), 4108-4110.
33. Kline, R. J.; McGehee, M. D.; Kadnikova, E. N.; Liu, J.; Fréchet, J. M.; Toney, M. F., Dependence of regioregular poly (3-hexylthiophene) film morphology and field-effect mobility on molecular weight. *Macromolecules* **2005,** *38* (8), 3312-3319.
34. Zen, A.; Saphiannikova, M.; Neher, D.; Grenzer, J.; Grigorian, S.; Pietsch, U.; Asawapirom, U.; Janietz, S.; Scherf, U.; Lieberwirth, I., Effect of molecular weight on the structure and crystallinity of poly (3-hexylthiophene). *Macromolecules* **2006,** *39* (6), 2162-2171.
35. Brinkmann, M.; Rannou, P., Molecular weight dependence of chain packing and semicrystalline structure in oriented films of regioregular poly (3-hexylthiophene) revealed by high-resolution transmission electron microscopy. *Macromolecules* **2009,** *42* (4), 1125-1130.
36. Mott, N., Conduction in glasses containing transition metal ions. *Journal of Non-Crystalline Solids* **1968,** *1* (1), 1-17.
37. Mott, N.; Davis, E., Electronic processes in non-crystalline materials, 2nd edn. Clarendon. Oxford: 1979.
38. Marcus, R. A., Chemical and electrochemical electron-transfer theory. *Annual review of physical chemistry* **1964,** *15*, 155-196.
39. Tassis, D.; Dimitriadis, C.; Valassiades, O., The Meyer–Neldel rule in the conductivity of polycrystalline semiconducting FeSi 2 films. *Journal of applied physics* **1998,** *84* (5), 2960-2962.
40. Guillen, C.; Herrero, J., Investigations of the electrical properties of electrodeposited CuInSe2 thin films. *Journal of applied physics* **1992,** *71* (11), 5479-5483.
41. Tassis, D.; Dimitriadis, C.; Brini, J.; Kamarinos, G.; Birbas, A., Low-frequency noise in polycrystalline semiconducting FeSi 2 thin films. *Journal of applied physics* **1999,** *85* (8), 4091-4095.
42. Paasch, G.; Lindner, T.; Scheinert, S., Variable range hopping as possible origin of a universal relation between conductivity and mobility in disordered organic semiconductors. *Synthetic Metals* **2002,** *132* (1), 97-104.
43. Dyre, J. C.; Schrøder, T. B., Universality of ac conduction in disordered solids. *Reviews of Modern Physics* **2000,** *72* (3), 873.
44. Duong, D. T.; Ho, V.; Shang, Z.; Mollinger, S.; Mannsfeld, S. C.; Dacuña, J.; Toney, M. F.; Segalman, R.; Salleo, A., Mechanism of crystallization and implications for charge transport in poly (3-ethylhexylthiophene) thin films. *Advanced Functional Materials* **2014,** *24* (28), 4515-4521.
45. Coropceanu, V.; Cornil, J.; da Silva Filho, D. A.; Olivier, Y.; Silbey, R.; Brédas, J.-L., Charge transport in organic semiconductors. *Chemical reviews* **2007,** *107* (4), 926-952.
46. Le Comber, P.; Spear, W., Electronic transport in amorphous silicon films. *Physical Review Letters* **1970,** *25* (8), 509.
47. Horowitz, G., Organic field-effect transistors. *Advanced materials* **1998,** *10* (5), 365-377.
48. Sirringhaus, H., Device physics of solution-processed organic field-effect transistors. *Advanced Materials* **2005,** *17* (20), 2411-2425.
49. Goh, C.; Kline, R. J.; McGehee, M. D.; Kadnikova, E. N.; Fréchet, J. M., Molecular-weight-dependent mobilities in regioregular poly (3-hexyl-thiophene) diodes. *Applied Physics Letters* **2005,** *86* (12), 122110.

50. Li, B.; Chen, J.; Zhao, Y.; Yang, D.; Ma, D., Effects of carrier trapping and scattering on hole transport properties of N, N′-diphenyl-N, N′-bis (1-naphthyl)-1, 1′-biphenyl-4, 4′-diamine thin films. *Organic Electronics* **2011,** *12* (6), 974-979.
51. Crine, J.-P., On the interpretation of some electrical aging and relaxation phenomena in solid dielectrics. *IEEE Transactions on Dielectrics and Electrical Insulation* **2005,** *12* (6), 1089-1107.
52. Qian, Z.; Cao, Z.; Galuska, L.; Zhang, S.; Xu, J.; Gu, X., Glass transition phenomenon for conjugated polymers. *Macromolecular Chemistry and Physics* **2019,** *220* (11), 1900062.
53. Ramos, J. J. M.; Diogo, H. P., The determination of the glass transition temperature by thermally stimulated depolarization currents. Comparison with the performance of other techniques. *Phase Transitions* **2017,** *90* (11), 1061-1078.
54. Kremer, F.; Schönhals, A., *Broadband dielectric spectroscopy*. Springer Science & Business Media: 2002.
55. Thomas, S.; Thomas, R.; Zachariah, A. K.; Mishra, R. K., *Spectroscopic methods for nanomaterials characterization*. Elsevier: 2017; Vol. 2.
56. McCrum, N. G.; Read, B. E.; Williams, G., *Anelastic and dielectric effects in polymeric solids*. John Wiley and Sons Ltd.: London, United Kingdom, 1967.
57. Obrzut, J.; Page, K. A., Electrical conductivity and relaxation in poly (3-hexylthiophene). *Physical Review B* **2009,** *80* (19), 195211.
58. Sirringhaus, H.; Brown, P.; Friend, R.; Nielsen, M. M.; Bechgaard, K.; Langeveld-Voss, B.; Spiering, A.; Janssen, R. A.; Meijer, E.; Herwig, P., Two-dimensional charge transport in self-organized, high-mobility conjugated polymers. *Nature* **1999,** *401* (6754), 685-688.
59. Shen, X.; Duzhko, V. V.; Russell, T. P., A Study on the Correlation Between Structure and Hole Transport in Semi-Crystalline Regioregular P3HT. *Advanced Energy Materials* **2013,** *3* (2), 263-270.
60. Abdou, M. S.; Orfino, F. P.; Son, Y.; Holdcroft, S., Interaction of oxygen with conjugated polymers: Charge transfer complex formation with poly (3-alkylthiophenes). *Journal of the American Chemical Society* **1997,** *119* (19), 4518-4524.
61. Khelifi, S.; Decock, K.; Lauwaert, J.; Vrielinck, H.; Spoltore, D.; Piersimoni, F.; Manca, J.; Belghachi, A.; Burgelman, M., Investigation of defects by admittance spectroscopy measurements in poly (3-hexylthiophene):(6, 6)-phenyl C61-butyric acid methyl ester organic solar cells degraded under air exposure. *Journal of Applied Physics* **2011,** *110* (9), 094509.
62. Uludağ, C.; Alveroglu, E.; Koç, K.; Karabul, Y.; Kılıç, M.; Özdemir, Z. G., Dielectric properties of P3HT/CSA composites for energy storage applications. *Physica B: Condensed Matter* **2022,** *626*, 413508.
63. Troisi, A.; Orlandi, G., Charge-transport regime of crystalline organic semiconductors: Diffusion limited by thermal off-diagonal electronic disorder. *Physical review letters* **2006,** *96* (8), 086601.
64. Kittel, C.; McEuen, P.; McEuen, P., *Introduction to solid state physics*. 8 ed.; Wiley New York: 1996.
65. Yelon, A.; Movaghar, B.; Crandall, R., Multi-excitation entropy: its role in thermodynamics and kinetics. *Reports on Progress in Physics* **2006,** *69* (4), 1145.

66. Meyer, W.; Neldel, H., Relation between the energy constant and the quantity constant in the conductivity–temperature formula of oxide semiconductors. *Z. tech. Phys* **1937,** *18* (12), 588-593.
67. Meyer, W. v.; Neldel, H., Relation between the energy constant and the quantity constant in the conductivity–temperature formula of oxide semiconductors. *Z. tech. Phys* **1937,** *18* (12), 588-593.
68. Lubianiker, Y.; Balberg, I., A comparative study of the Meyer–Neldel rule in porous silicon and hydrogenated amorphous silicon. *Journal of non-crystalline solids* **1998,** *227*, 180-184.
69. Overhof, H.; Thomas, P., Electronic Transport in Hydrogenated Amorphous Semiconductors, Springer-Verlag, Berlin 1989.
70. Kondo, M.; Chida, Y.; Matsuda, A., Observation of Meyer-Neldel rule in extended energy regime using novel a-Si: H TFTs. *Journal of non-crystalline solids* **1996,** *198*, 178-181.
71. Ram, S. K.; Kumar, S.; Vanderhaghen, R.; i Cabarrocas, P. R., Investigations of the electron transport behavior in microcrystalline Si films. *Journal of non-crystalline solids* **2002,** *299*, 411-415.
72. Linert, W.; Jameson, R., The isokinetic relationship. *Chemical Society Reviews* **1989,** *18*, 477-505.
73. Keyes, R. W., Volumes of activation for diffusion in solids. *The Journal of Chemical Physics* **1958,** *29* (3), 467-475.
74. Rosenberg, B.; Kemeny, G.; Switzer, R. C.; Hamilton, T. C., Quantitative evidence for protein denaturation as the cause of thermal death. *Nature* **1971,** *232* (5311), 471-473.
75. Jaoul, O.; Sautter, V., A new approach to geospeedometry based on thecompensation law'. *Physics of the earth and planetary interiors* **1999,** *110* (1-2), 95-114.
76. Stallinga, P., Electronic transport in organic materials: Comparison of band theory with percolation/(variable range) hopping theory. *Advanced Materials* **2011,** *23* (30), 3356-3362.
77. Elliott, S., Ac conduction in amorphous chalcogenide and pnictide semiconductors. *Advances in physics* **1987,** *36* (2), 135-217.
78. Pivrikas, A.; Ullah, M.; Singh, T. B.; Simbrunner, C.; Matt, G.; Sitter, H.; Sariciftci, N., Meyer–Neldel rule for charge carrier transport in fullerene devices: a comparative study. *Organic electronics* **2011,** *12* (1), 161-168.
79. Fishchuk, I. I.; Kadashchuk, A.; Mityashin, A.; Gavrilyuk, M.; Köhler, A.; Bässler, H.; Genoe, J.; Sitter, H.; Sariciftci, N., Origin of Meyer-Neldel type compensation behavior in organic semiconductors at large carrier concentrations: Disorder versus thermodynamic description. *Physical Review B* **2014,** *90* (24), 245201.
80. Fishchuk, I.; Kadashchuk, A.; Genoe, J.; Ullah, M.; Sitter, H.; Singh, T. B.; Sariciftci, N.; Bässler, H., Temperature dependence of the charge carrier mobility in disordered organic semiconductors at large carrier concentrations. *Physical Review B* **2010,** *81* (4), 045202.
81. Linert, W., A result of resonant energy exchange between reactants and their chemical surrounding: The isokinetic relationship. *Collection of Czechoslovak chemical communications* **1990,** *55* (1), 21-31.
82. Yelon, A.; Movaghar, B., Microscopic explanation of the compensation (Meyer-Neldel) rule. *Physical review letters* **1990,** *65* (5), 618.
83. Yelon, A.; Movaghar, B.; Branz, H., Origin and consequences of the compensation (Meyer-Neldel) law. *Physical Review B* **1992,** *46* (19), 12244.

84. Du, P.; Li, N.; Ling, X.; Fan, Z.; Braun, A.; Yang, W.; Chen, Q.; Yelon, A., Optimizing the Proton Conductivity with the Isokinetic Temperature in Perovskite-Type Proton Conductors According to Meyer–Neldel Rule. *Advanced Energy Materials* **2022,** *12* (5), 2102939.
85. Shimakawa, K.; Abdel-Wahab, F., The Meyer–Neldel rule in chalcogenide glasses. *Applied physics letters* **1997,** *70* (5), 652-654.
86. Yelon, A.; Movaghar, B., The Meyer–Neldel conductivity prefactor for chalcogenide glasses. *Applied physics letters* **1997,** *71* (24), 3549-3551.
87. Irsigler, P.; Wagner, D.; Dunstan, D., On the application of the Meyer-Neldel rule to a-Si: H. *Journal of Physics C: Solid State Physics* **1983,** *16* (34), 6605.
88. Yakimov, A. I. e.; Dvurechenskii, A. V. e.; Nikiforov, A.; Mikhalev, G. Y., The Meyer-Neldel rule in the processes of thermal emission and hole capture in Ge/Si quantum dots. *Journal of Experimental and Theoretical Physics Letters* **2004,** *80* (5), 321-325.
89. Coutts, T.; Pearsall, N., Meyer–Neldel rule in solar cells. *Applied Physics Letters* **1984,** *44* (1), 134-135.
90. Boisvert, G.; Lewis, L. J.; Yelon, A., Many-body nature of the Meyer-Neldel compensation law for diffusion. *Physical review letters* **1995,** *75* (3), 469.
91. Gelin, S.; Champagne-Ruel, A.; Mousseau, N., Enthalpy-entropy compensation of atomic diffusion originates from softening of low frequency phonons. *Nature communications* **2020,** *11* (1), 1-7.
92. Yelon, A., The fallacy of Meyer-Neldel temperature as a measure of disorder. *Monatshefte für Chemie-Chemical Monthly* **2013,** *144* (1), 91-95.
93. Fortner, J.; Karpov, V.; Saboungi, M. L., Meyer–Neldel rule for liquid semiconductors. *Applied physics letters* **1995,** *66* (8), 997-999.
94. Newman, C. R.; Frisbie, C. D.; da Silva Filho, D. A.; Brédas, J.-L.; Ewbank, P. C.; Mann, K. R., Introduction to organic thin film transistors and design of n-channel organic semiconductors. *Chemistry of materials* **2004,** *16* (23), 4436-4451.
95. Mehta, N., Meyer–Neldel rule in chalcogenide glasses: Recent observations and their consequences. *Current Opinion in Solid State and Materials Science* **2010,** *14* (5), 95-106.
96. Lee, J.-S.; Kovalenko, M. V.; Huang, J.; Chung, D. S.; Talapin, D. V., Band-like transport, high electron mobility and high photoconductivity in all-inorganic nanocrystal arrays. *Nature nanotechnology* **2011,** *6* (6), 348-352.
97. Cazaux, J., Recent developments and new strategies in scanning electron microscopy. *Journal of microscopy* **2005,** *217* (1), 16-35.
98. Akhtar, K.; Khan, S. A.; Khan, S. B.; Asiri, A. M., Scanning electron microscopy: Principle and applications in nanomaterials characterization. In *Handbook of materials characterization*, Springer: 2018; pp 113-145.
99. Ladd, M. F. C.; Palmer, R. A.; Palmer, R. A., *Structure determination by X-ray crystallography*. Springer: 1977; Vol. 233.
100. Li, Y.; Sonar, P.; Murphy, L.; Hong, W., High mobility diketopyrrolopyrrole (DPP)-based organic semiconductor materials for organic thin film transistors and photovoltaics. *Energy & Environmental Science* **2013,** *6* (6), 1684-1710.
101. Chauhan, A.; Chauhan, P., Powder XRD technique and its applications in science and technology. *J Anal Bioanal Tech* **2014,** *5* (5), 1-5.

102. Meijer, E.; Matters, M.; Herwig, P.; De Leeuw, D.; Klapwijk, T., The Meyer–Neldel rule in organic thin-film transistors. *Applied Physics Letters* **2000,** *76* (23), 3433-3435.
103. Koch, F. P. V.; Rivnay, J.; Foster, S.; Müller, C.; Downing, J. M.; Buchaca-Domingo, E.; Westacott, P.; Yu, L.; Yuan, M.; Baklar, M., The impact of molecular weight on microstructure and charge transport in semicrystalline polymer semiconductors–poly (3-hexylthiophene), a model study. *Progress in polymer science* **2013,** *38* (12), 1978-1989.
104. Dixon, A. G.; Visvanathan, R.; Clark, N. A.; Stingelin, N.; Kopidakis, N.; Shaheen, S. E., Molecular weight dependence of carrier mobility and recombination rate in neat P3HT films. *Journal of Polymer Science Part B: Polymer Physics* **2018,** *56* (1), 31-35.
105. Xie, R.; Lee, Y.; Aplan, M. P.; Caggiano, N. J.; Müller, C.; Colby, R. H.; Gomez, E. D., Glass transition temperature of conjugated polymers by oscillatory shear rheometry. *Macromolecules* **2017,** *50* (13), 5146-5154.
106. Fox Jr, T. G.; Flory, P. J., Second-order transition temperatures and related properties of polystyrene. I. Influence of molecular weight. *Journal of Applied Physics* **1950,** *21* (6), 581-591.
107. Ballantyne, A. M.; Chen, L.; Dane, J.; Hammant, T.; Braun, F. M.; Heeney, M.; Duffy, W.; McCulloch, I.; Bradley, D. D.; Nelson, J., The effect of poly (3-hexylthiophene) molecular weight on charge transport and the performance of polymer: fullerene solar cells. *Advanced Functional Materials* **2008,** *18* (16), 2373-2380.
108. Abdel-Wahab, F., Signature of the Meyer–Neldel rule on the correlated barrier-hopping model. *Journal of applied physics* **2002,** *91* (1), 265-270.
109. Pike, G., AC conductivity of scandium oxide and a new hopping model for conductivity. *Physical Review B* **1972,** *6* (4), 1572.
110. Abdel-Wahab, F.; Montaser, A.; Yelon, A., Mechanism of ac and dc conduction in chalcogenide glasses. *Monatshefte für Chemie-Chemical Monthly* **2013,** *144* (1), 83-89.
111. Crine, J. P., A new analysis of the results of thermally stimulated measurements in polymers. *Journal of applied physics* **1989,** *66* (3), 1308-1313.
112. Gu, K.; Wang, Y.; Li, R.; Tsai, E.; Onorato, J. W.; Luscombe, C. K.; Priestley, R. D.; Loo, Y.-L., Role of Postdeposition Thermal Annealing on Intracrystallite and Intercrystallite Structuring and Charge Transport in Poly (3-hexylthiophene). *ACS Applied Materials & Interfaces* **2020,** *13* (1), 999-1007.
113. Van Turnhout, J., Thermally stimulated discharge of polymer electrets. *Polymer Journal* **1971,** *2* (2), 173-191.
114. Bässler, H.; Köhler, A., Charge transport in organic semiconductors. In *Unimolecular and supramolecular electronics I*, Springer: 2011; pp 1-65.
115. Groves, C., Simulating charge transport in organic semiconductors and devices: a review. *Reports on Progress in Physics* **2016,** *80* (2), 026502.
116. Fishchuk, I.; Kadashchuk, A.; Genoe, J.; Poroshin, V.; Bässler, H., Does the Temperature Dependence of the Charge Carrier Mobility in Disordered Organic Semiconductors at Large Carrier Concentrations Obey the Meyer–Neldel Compensation Law? *Molecular Crystals and Liquid Crystals* **2011,** *535* (1), 1-9.
117. Von Hauff, E. Field effect investigations of charge carrier transport in organic semiconductors. Universität Oldenburg, 2006.
118. Chua, L.-L.; Zaumseil, J.; Chang, J.-F.; Ou, E. C.-W.; Ho, P. K.-H.; Sirringhaus, H.; Friend, R. H., General observation of n-type field-effect behaviour in organic semiconductors. *Nature* **2005,** *434* (7030), 194-199.

119. Zhang, Y.; Yip, H.-L.; Acton, O.; Hau, S. K.; Huang, F.; Jen, A. K.-Y., A simple and effective way of achieving highly efficient and thermally stable bulk-heterojunction polymer solar cells using amorphous fullerene derivatives as electron acceptor. *Chemistry of Materials* **2009,** *21* (13), 2598-2600.
120. Yang, X.; van Duren, J. K.; Rispens, M. T.; Hummelen, J. C.; Janssen, R. A.; Michels, M. A.; Loos, J., Crystalline organization of a methanofullerene as used for plastic solar-cell applications. *Advanced Materials* **2004,** *16* (9-10), 802-806.
121. Lan, T.; Soavi, F.; Marcaccio, M.; Brunner, P.-L.; Sayago, J.; Santato, C., Electrolyte-gated transistors based on phenyl-C 61-butyric acid methyl ester (PCBM) films: bridging redox properties, charge carrier transport and device performance. *Chemical Communications* **2018,** *54* (43), 5490-5493.
122. Erb, T.; Zhokhavets, U.; Gobsch, G.; Raleva, S.; Stühn, B.; Schilinsky, P.; Waldauf, C.; Brabec, C. J., Correlation between structural and optical properties of composite polymer/fullerene films for organic solar cells. *Advanced Functional Materials* **2005,** *15* (7), 1193-1196.
123. Chen, S.; Li, Z.; Qiao, Y.; Song, Y., Solution-processed organic semiconductor crystals for field-effect transistors: from crystallization mechanism towards morphology control. *Journal of Materials Chemistry C* **2021,** *9* (4), 1126-1149.
124. Lee, S. S.; Kim, C. S.; Gomez, E. D.; Purushothaman, B.; Toney, M. F.; Wang, C.; Hexemer, A.; Anthony, J. E.; Loo, Y. L., Controlling nucleation and crystallization in solution-processed organic semiconductors for thin-film transistors. *Advanced Materials* **2009,** *21* (35), 3605-3609.
125. Jiang, H.; Kloc, C., Single-crystal growth of organic semiconductors. *MRS bulletin* **2013,** *38* (1), 28-33.
126. Würthner, F.; Schmidt, R., Electronic and Crystal Engineering of Acenes for Solution-Processible Self-Assembling Organic Semiconductors. *Chemphyschem: a European journal of chemical physics and physical chemistry* **2006,** *7* (4), 793-797.
127. Zhong, Y.; Suzuki, K.; Inoue, D.; Hashizume, D.; Izawa, S.; Hashimoto, K.; Koganezawa, T.; Tajima, K., Interface-induced crystallization and nanostructure formation of [6, 6]-phenyl-C 61-butyric acid methyl ester (PCBM) in polymer blend films and its application in photovoltaics. *Journal of Materials Chemistry A* **2016,** *4* (9), 3335-3341.
128. Gupta, R. K.; Das, D.; Gupta, M.; Pal, S. K.; Iyer, P. K.; Achalkumar, A. S., Electroluminescent room temperature columnar liquid crystals based on bay-annulated perylene tetraesters. *Journal of Materials Chemistry C* **2017,** *5* (7), 1767-1781.
129. Shelar, P. S., A critical review and finite element study of structural relaxation in veneered 3Y-TZP dental structures. **2021**.
130. Zhang, W.; Sathitsuksanoh, N.; Simmons, B. A.; Frazier, C. E.; Barone, J. R.; Renneckar, S., Revealing the thermal sensitivity of lignin during glycerol thermal processing through structural analysis. *RSC advances* **2016,** *6* (36), 30234-30246.
131. Ariesandi, W.; Chang, C.-F.; Chen, T.-E.; Chen, Y.-R., Temperature-dependent structural changes of Parkinson's alpha-synuclein reveal the role of pre-existing oligomers in alpha-synuclein fibrillization. *PLoS One* **2013,** *8* (1), e53487.

132. Gupta, R. K.; Pathak, S. K.; Pradhan, B.; Rao, D. S.; Prasad, S. K.; Achalkumar, A. S., Self-assembly of luminescent N-annulated perylene tetraesters into fluid columnar phases. *Soft Matter* **2015,** *11* (18), 3629-3636.
133. Nowak-Król, A.; Würthner, F., Progress in the synthesis of perylene bisimide dyes. *Organic Chemistry Frontiers* **2019,** *6* (8), 1272-1318.

APPENDIX A LIST OF PUBLICATIONS IN POLYTECHNIQUE MONTREAL NOT INCLUDED IN THE THESIS

[1] Lan, T., Gao, Z., Barbosa, M. and Santato, C., Flexible Ion-Gated Transistors Making Use of Poly-3-hexylthiophene (P3HT): Effect of the Molecular Weight on the Effectiveness of Gating and Device Performance, J. Electron. Mater. 2020, 49, 5302-5307.

[2] Gao, Z., Niyonkuru, D., Yelon, A. and Santato, C., Charge carrier transport in a small molecule organic semiconductor: Phenyl-C61-butyric acid methyl ester (PCBM), In submission.

[3] Cecchi, T., Gao, Z., Clement, C., Girard, O., Karim, A. and Santato, C., Sustainable and logical gold peeling from e-waste via food waste byproducts, Nanotechnology, under revision.

APPENDIX B PARTICIPATION IN CONFERENCES

1. IEEE summer school, 2017, Montreal.

2. Innovation 360, Nano Canada, 2017, Montreal.

3. “Charge carrier transport in a polymeric semiconductor: Poly(3-hexylthiophene-2,5-diyl) (P3HT)” Materials Research Society (MRS) Fall Meeting and Exhibit, 2019, Boston, Poster presentation.

4. “Dependence of Charge Carrier Transport on Molecular Relaxations in Glassy Conducting Polymer” Green Electronics Network Symposium, 2022, Montreal, Poster presentation.

5. “Dependence of charge carrier transport on backbone molecular relaxations in organic electronic polymers” American Chemical Society (ACS) Fall, 2022, Chicago, Oral presentation.